TRANSITORY STATIC AND KINETIC BOUNDARY FRICTION MECHANISMS

by

TERENCE LIONEL MARION

B.A.Sc., University of British Columbia,
Vancouver, British Columbia, 1967

A THESIS SUBMITTED IN PARTIAL FULFILMENT OF
THE REQUIREMENTS FOR THE DEGREE OF
DOCTOR OF PHILOSOPHY

in the Department
of
Mechanical Engineering

We accept this thesis as conforming to the
required standard

THE UNIVERSITY OF BRITISH COLUMBIA

June, 1972

In presenting this thesis in partial fulfilment of the requirements for an advanced degree at the University of British Columbia, I agree that the Library shall make it freely available for reference and study. I further agree that permission for extensive copying of this thesis for scholarly purposes may be granted by the Head of my Department or by his representatives. It is understood that copying or publication of this thesis for financial gain shall not be allowed without my written permission.

TERENCE LIONEL MARION

Department of MECHANICAL ENGINEERING

The University of British Columbia
Vancouver 8, Canada

Date SEPTEMBER 27, 1972

ABSTRACT

The purpose of the investigation was to study, by analysis of friction-induced vibration, the underlying physical mechanisms of metallic boundary friction. Dynamic system response and interfacial friction force data, from a pin-on-disc machine operating over a broad range of surface speeds, was electronically monitored and photographically recorded. Excellent agreement in the response curve profiles of recorded rate-sensitive static friction data and a predictive curve developed by assumption of a plastic deformation model of contact area growth suggests strongly that plastic deformation is indeed the controlling physical mechanism of metallic static friction. The existence of an upper asymptote of static friction in the presence of a lubricant, and the existence in the "slip" friction curve of a transient which appears governed by the relative dynamic displacement of the surfaces, has been proven. Vibratory slip and quasi-harmonic oscillation both exhibited simultaneous solid-contact and viscous fluid film characteristics. The "humped" form of friction force vs velocity curve necessary for quasi-harmonic oscillation was concluded to differ from that of non-oscillatory slip only because of thermal variation in the fluid viscosity, similar to that encountered in elastohydrodynamic studies.

In every instance rate effects were found to determine or profoundly influence the physical mechanisms of metallic boundary friction.

ACKNOWLEDGEMENT

Sincere thanks are extended to Mr. E. Jones, Tribology Laboratory technician, for his knowledgeable advice concerning practical development of the experimental apparatus, as well as for the construction of the instrumentation circuitry. His assistance was truly invaluable. The author wishes to acknowledge the support and constructive criticism tendered him by Dr. C.A. Brockley, and to thank his associates in the laboratory for the opportunity to participate in fruitful discussion.

Equipment constructed by the author's predecessors, Dr. H.R. Davis and Dr. P.L. Ko, greatly reduced the task of preparing suitable experimental apparatus: the time so saved is not unappreciated.

The experimental investigation was performed in the Tribology Laboratory, Department of Mechanical Engineering, University of British Columbia. Financial assistance, in the form of NRC Bursaries, was received from the National Research Council of Canada.

TABLE OF CONTENTS

LIST OF ILLUSTRATIONS

NOTATION

Symbol	Description	Units
A, A_s, $\dot{A}_s$	total area of actual contact at the interface of two surfaces, area of actual contact at inception of slip, and rate of change of area of contact at inception of slip, respectively	in^2
E_1, E_2	modulii of elasticity of steel and aluminum, respectively	lb/in^2
F, F_s, $\dot{F}_s$	total tangential load at interface of friction surfaces, interfacial tangential load at inception of slip, and rate of change of tangential load at inception of slip, respectively	lb
I_1, I_2	area moments of inertia of portions of composite cantilever beam	in^4
J	work equivalent of heat	in-lb/BTU
K	constant of proportionality	
L_1, L_2	lengths of portions of composite cantilever beam	in
M	dynamic equivalent mass of slider and supporting structure	$lb\text{-}sec^2/in$
N_f	normal load supported by fluid pressure	lb
N_s	normal load supported by solid contact	lb
P	applied load	lb
R	radius of slider	in
S_1, S_2, S_3	principal stresses	lb/in^2
T	temperature	^oF
U	velocity of slider in x direction relative to lower surface, $(\dot{x} - v)$	in/sec

Symbol	Description	Units
V	velocity of slider in y direction	in/sec
W	total normal load at frictional interface	lb
Y	yield stress of ductile material in uniaxial tension	lb/in^2
a, b	constants of proportionality	
g	acceleration of gravity	in/sec^2
h	thickness of liquid lubricant layer	in
$h(\sigma)$	activation enthalpy	BTU
k	stiffness of composite cantilever beam	lb/in
k_1, k_2	linearly elastic stiffness coefficients	lb/in
m, n	constants of proportionality	
p	local static pressure in liquid lubricant	lb/in^2
r, r_c	actual and critical viscous dissipation coefficients for elastically-restrained slider, respectively	lb-sec/in
t, t_s	time, and time duration of stick portion of stick-slip cycle, respectively	sec
u	velocity of lubricant in x direction	in/sec
v	velocity of lower surface	in/sec
x, $\dot{x}$, $\ddot{x}$	displacement, velocity, and acceleration of slider, respectively, in plane of frictional interface	
y	normal to frictional interface	
z	co-ordinate normal to x-y plane	

Symbol	Description	Units
α, β	constants of proportionality	
γ	coefficient of viscosity variation with temperature	$^{\circ}F^{-1}$
Δ	length of rectangular load-carrying film	in
δ, $\dot{\delta}$	elastic extension/deflection from equilibrium length/position and rate of change of extension/deflection, respectively	
$\dot{\varepsilon}$	rate of strain in uniaxial tension	sec^{-1}
η	viscosity of liquid lubricant	$lb\text{-}sec/in^2$
θ	angular displacement	rad
λ	width of rectangular load-carrying film	in
μ_k, μ_k'	kinetic friction coefficient and value of kinetic friction coefficient at which transitory kinetic friction curve meets stable kinetic friction curve, respectively	
μ_s, $\dot{\mu}_s$	coefficient of friction at inception of slip and rate of change of coefficient of friction at inception of slip, respectively	
ξ	thermal conductivity	BTU/in-sec-°F
ρ	radial co-ordinate in cylindrical co-ordinate system	
σ_0	compressive stress required to produce complete plastic yielding over true area of contact	lb/in^2
σ_y	normal stress at frictional interface, W/A	lb/in^2
τ_i, τ_0	plastic shear strength of interfacial junction, F_s/A_s, and plastic shear strength of bulk material, respectively	lb/in^2

Symbol	Description	Units
τ_{yx}, $\dot{\tau}_{yx}$	tangential shear stress at frictional interface, F/A, and rate of change of tangential shear stress at frictional interface	
$\dot{\phi}$	load rate variable, $\dot{\tau}_{yx}/\sigma_y$	sec^{-1}
ψ	coefficient of viscosity variation with pressure	in^2/lb
ω_n, ω_d	undamped natural frequency of vibration and damped natural frequency of vibration, respectively	rad/sec

CHAPTER I

I. INTRODUCTION

Boundary friction may be defined as resistance to motion which occurs when two solid bodies are in physical contact under the influence of an applied tangential stress. The nature of the opposing surfaces is therefore of paramount importance to any discussion of such frictional action.

No matter how well finished, all engineering surfaces are extremely rough on a microscopic scale. Thus, when two nominally flat surfaces are brought together they touch only at their extremities, and their frictional behavior is dominated by the properties of these small regions of contact. These microscopic extremities are commonly called asperities.

Upon considering the present knowledge of physical and chemical properties of materials, one might suppose the nature of frictional interaction between contacting surfaces to be well understood. The converse is true. Not only is the actual mechanism of friction in doubt; predictions of boundary friction coefficient values cannot be made, even empirically, with any notable degree of accuracy. So many variables affect frictional behavior that investigators concur only in that surfaces in contact meet at opposing asperities, and that these asperities deform, either elastically or plastically, under load.

When one member of a boundary friction pair is elastically restrained, and the other member given a velocity relative to the point of restraint (Fig. 1.1.1), oscillation of the elastically-restrained member, commonly called "friction-induced vibration", frequently occurs. This oscillation is of considerable engineering interest, in its own right, since it considerably increases wear, and detracts from the accuracy and reliability of mechanisms and measuring devices. But, for purposes of the present study, the significance of such oscillation is that it may be used by investigators in search of greater insight into the phenomena of boundary friction.

Two forms of friction-induced vibration are recognized (Fig. 1.1.2). "Stick-slip vibration" is characterized by a saw-tooth form of displacement vs time plot, whereas "quasi-harmonic vibration" exhibits a displacement vs time waveform that is near-sinusoidal. During stick-slip vibration the elastically-restrained member "sticks" to the driven member, causing the displacement of the restrained member to increase until the restraining force exceeds the maximum "static" friction force which the interfacial surface is capable of sustaining. The restrained member then decreases its displacement, under the influence of "kinetic" friction forces, until it once again achieves zero velocity with respect to the driven surface. During quasi-harmonic vibration, which occurs at higher driven-surface speeds

than stick-slip vibration, relative velocity between the surfaces always exceeds zero.

Both forms of friction-induced vibration have received substantial documentation, but usually with the emphasis on definition of the vibratory behaviour. The friction mechanisms causing the vibration, which have general applicability to boundary friction as a whole, are still inadequately understood, largely because the presence of the frictional oscillations has obscured the form of the friction forces responsible for the oscillation. Further investigation of these physical mechanisms of friction was consequently considered attention well directed.

In the course of this study the plastic deformation model of Tabor will be extended to include the effect of rate of application of tangential load, and the results compared to static friction data collected by monitoring friction-induced vibration. The dynamic friction force recordings obtained by monitoring the vibration will also be analyzed. Minimized chemical effects will be neglected; the only concern of the present investigation will be the physical phenomena relevant to friction of metallic surfaces.

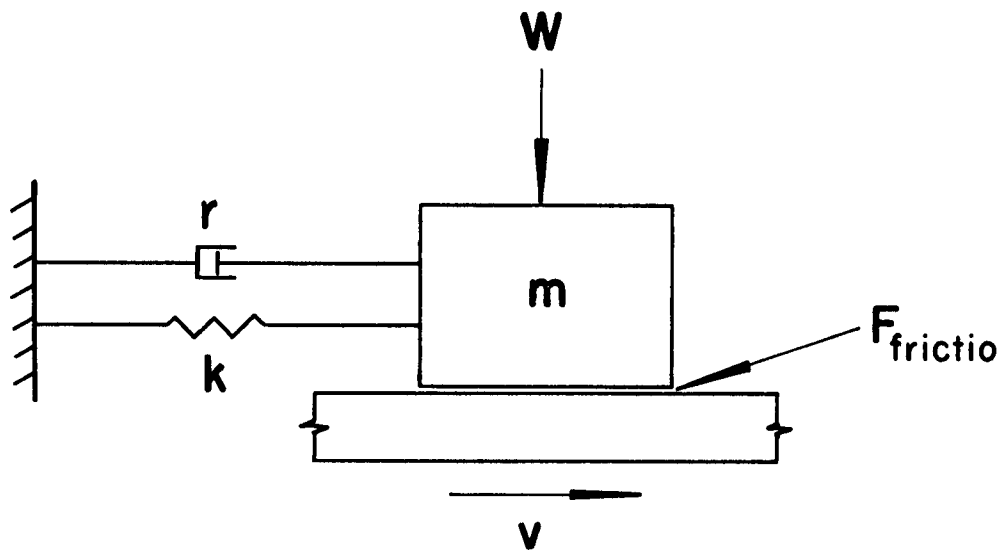

Figure 1.1.1 Schematic System Required for Incidence of Friction-Induced Oscillation

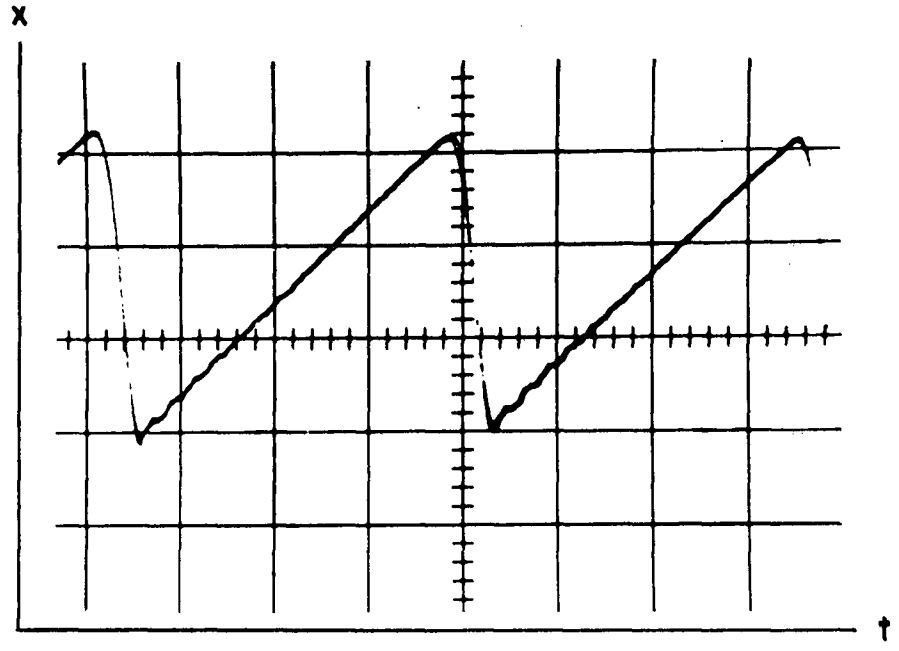

(a) STICK-SLIP

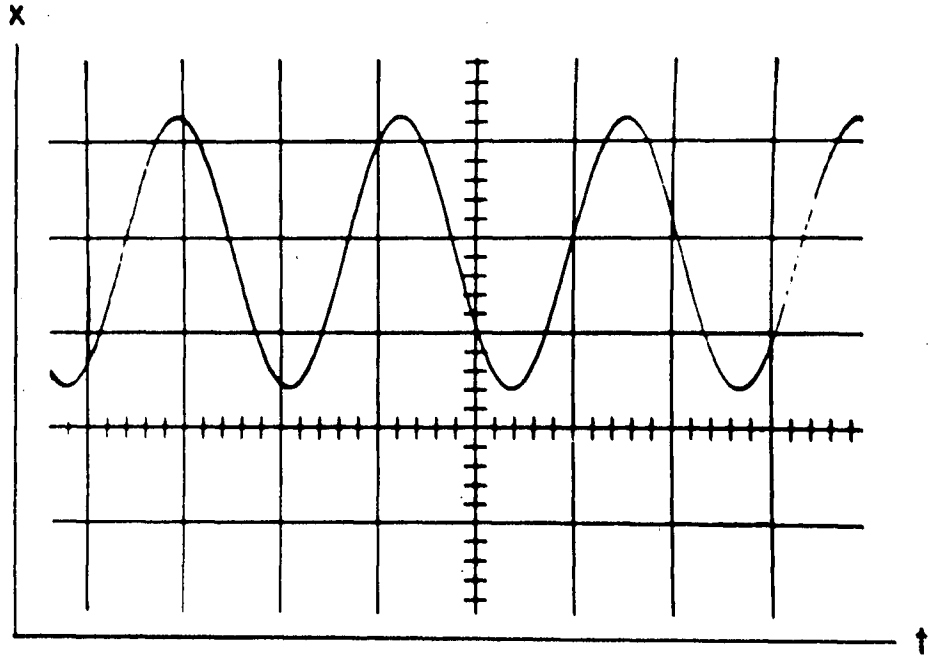

(b) QUASI-HARMONIC

Figure 1.1.2 Displacement vs Time Waveforms of the Two Forms of Friction-Induced Oscillation (Ko)

CHAPTER II

II. HISTORICAL BACKGROUND

Although friction-induced vibration is a very common phenomenon, only in recent years have the friction forces causing the vibration been subjected to serious investigation. In fact, it was not until 1930 that an investigator, Thomas [1], reported an analytic investigation of friction-induced vibration using graphical techniques. He erroneously concluded that the phenomenon we presently call quasi-harmonic oscillation was simply totally undamped simple harmonic motion, with the static friction force as the initial condition. He did, however, even assuming a constant value for the kinetic friction coefficient, correctly conclude that stick-slip oscillation occurs only if the interfacial kinetic friction coefficient is less than the static friction coefficient, and even then, only if the damping forces are of less than a critical magnitude.

Papenhuyzen [2], in 1938, investigating the skidding of automobile tires, was first to demonstrate that stick-slip oscillation and quasi-harmonic oscillation can occur under similar frictional conditions, but at different velocities of the driven surface.

Bowden and Leben [3], in 1939, reported that sliding velocities during the slip portion of stick-slip oscillation were very high, in comparison to the driven surface velocity,

and suggested that localized welding could occur at the termination of the slip portion of a cycle as a result of high-temperature flashes at opposing asperities. This suggestion was based on experiments by Bowden and Ridler [4], reported in 1936, in which interfacial temperature between two metal surfaces was investigated as a function of relative velocity, both with and without the application of lubricants. Peak local temperatures at the surface were, in all cases, found to rise with speed, to an upper limit equal numerically to the melting point of the softer metal.

Bristow [5], in 1945, stated that a necessary condition for the occurrence of stick-slip oscillation is the existence of a negative kinetic friction force vs velocity relationship, but offered no evidence to support this hypothesis. He did, however, demonstrate the existence of micro-displacement during the stick portion of the cycle.

Dudley and Swift [6], in 1949, reported the development of a simple graphical technique for determining the vibration cycle, on the phase plane, from any friction force vs velocity curve, and the application of this technique to analyze stick-slip vibration. Various forms of friction-force vs velocity curves were explored, with the static friction coefficient assumed equal to the kinetic friction coefficient extrapolated to zero velocity. They erroneously concluded that the amplitude of stick-slip vibration should increase with driven-surface velocity.

Bowden and Tabor [7], in 1950, proposed that metallic static friction is caused by localized adhesion, resulting from plastic deformation, of contacting surfaces. The area of contact was thereby a function of both normal and tangential loading; it would increase with either form of load. This theory, which offered creditable explanations for many observed metallic contact phenomena, was well received. Tabor subsequently extended the theory [22] to an impressive mathematical treatment of static friction, but the known influence of rate effects on observed coefficients of static friction was still unexplained.

Rabinowicz [8], in 1957, concluded that the amplitude of stick-slip oscillation is governed by the time duration of the stick portion of the cycle, and that the amplitude of quasi-harmonic oscillation is governed by the velocity of the driven surface.

Courtney-Pratt and Eisner [9], in 1957, showed that the growth of actual contact area under the influence of increasing tangential load was unaffected by the addition of liquid lubricants. The sole effect of the lubricants was to decrease the value of tangential load at which slip occurred.

Potter [10], in 1962, reported experimental results in which, contrary to Dudley and Swift's predictions, the amplitude of stick-slip vibration decreased with increasing velocity.

Cameron [11], in 1963, reported an analysis of stick-slip oscillation in which he assumed a linearly negative friction force vs velocity relationship (Fig. 2.1.1). Experimentally-measured amplitudes were reported in agreement with those predicted by the analysis.

Bell and Burdekin [12], in 1966, reported that by summation of electrical instrumentation signals they were able to record the interfacial kinetic friction force throughout the duration of a stick-slip cycle. Contrary to the various assumptions of all previous investigators, they found that the friction force was not a single-valued function of the interfacial velocity (Fig. 2.1.2). No explanation of these results was offered.

Davis [13], in 1966, reported that the behaviour of eleven metals, tested on a steel driven surface, was similar with respect to variation of the coefficient of static friction with driven surface velocity.

Johannes [14], in 1969, demonstrated conclusively that the amplitude of stick-slip vibration is not governed by the time of contact during the stick portion of the cycle, a misconception popular with many investigators at that time. He showed, rather, using the experimental data of Potter [10], that the coefficient of static friction can be correlated to the rate of application of shear stress, divided by the existing normal stress, at the interface. Johannes also proposed a simple visco-elastic mathematical model of asperity

junction growth, but did not achieve good correlation between the model and his experimental data.

Ko [15], in 1969, reported that quasi-harmonic oscillation is characterized by the presence of a "humped" form of single-valued friction force vs velocity curve (Fig. 2.1.3). The investigation utilized an improved version of the electronic summation techniques of Bell and Burdekin [12].

Green [16], in 1971, after studying stick-slip vibration, reported several interesting results. Massive seizure, rather than stick-slip oscillation, would occur, in air, when the major portion of surface contaminants was removed from the friction surfaces. The electrical conductivity between surfaces was found to increase non-linearly with tangential load (Fig. 2.1.4), and no substantial increases in conductivity were noted if the application of tangential load was arrested during the stick portion of a stick-slip cycle (Fig. 2.1.5).

Of particular interest to this study is the diversity of relationships, proposed by former researchers, expressing the coefficient of static friction achieved as a function of the time duration of the stick portion of a stick-slip cycle. The relationships are of three general forms.

$$\mu_s - \mu_k = \frac{at_s}{b + t_s}$$ Derjaguin, Push, and Tolstoi [17]

$$\frac{\mu_s - \mu_k}{\mu_{s_\infty} - \mu_k} = 1 - e^{-at_s}$$ Kosterin and Kragelskii [18]

$$\mu_s - \mu_k = at_s^b$$ Rabinowicz [8]
Davis [13]

These relationships are all, at best, semi-empirical. The formulation proposed by Rabinowicz and Davis predicted infinite coefficients of static friction for infinite duration of the stick portion of a cycle; the other equations, though dissimilar, predicted an upper asymptote for the static friction coefficient. This basic difference in concept has endured for several years, because none of these investigators collected data which could prove or disprove the presence of this upper asymptote.

Obviously, the investigation of physical boundary friction phenomena applicable to friction-induced oscillation has not, to date, achieved a high level of sophistication. Even which variables are of significance to such phenomena is not certain. The purpose of the present study is, by analysis of friction-induced vibration, to improve the current comprehension of the operative physical mechanisms of static and kinetic boundary friction of metals.

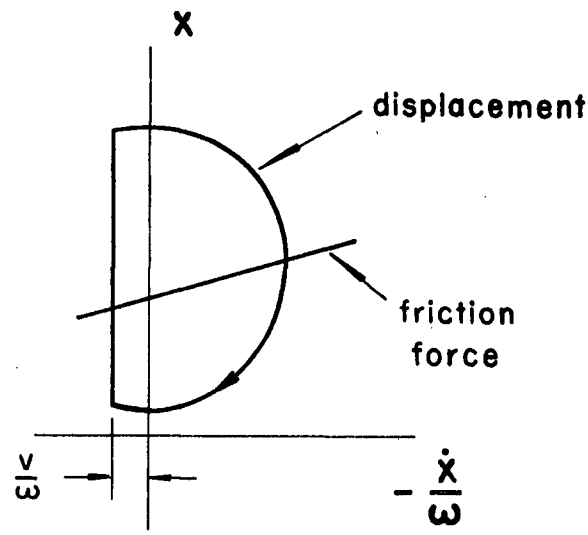

Figure 2.1.1 Assumed Linearly Negative Kinetic Friction vs Velocity Relationship of Cameron, with Generated Phase Plane Behavioural Trace

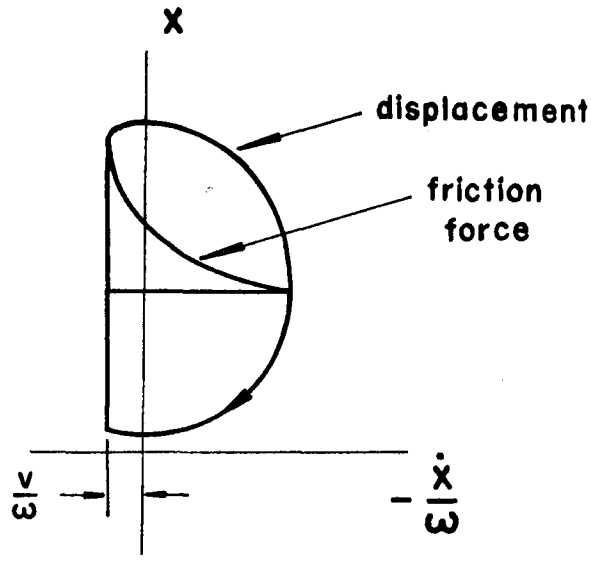

Figure 2.1.2 Kinetic Friction vs Velocity Relationship Recorded Experimentally by Bell and Burdekin, with Generated Phase Plane Behavioural Trace

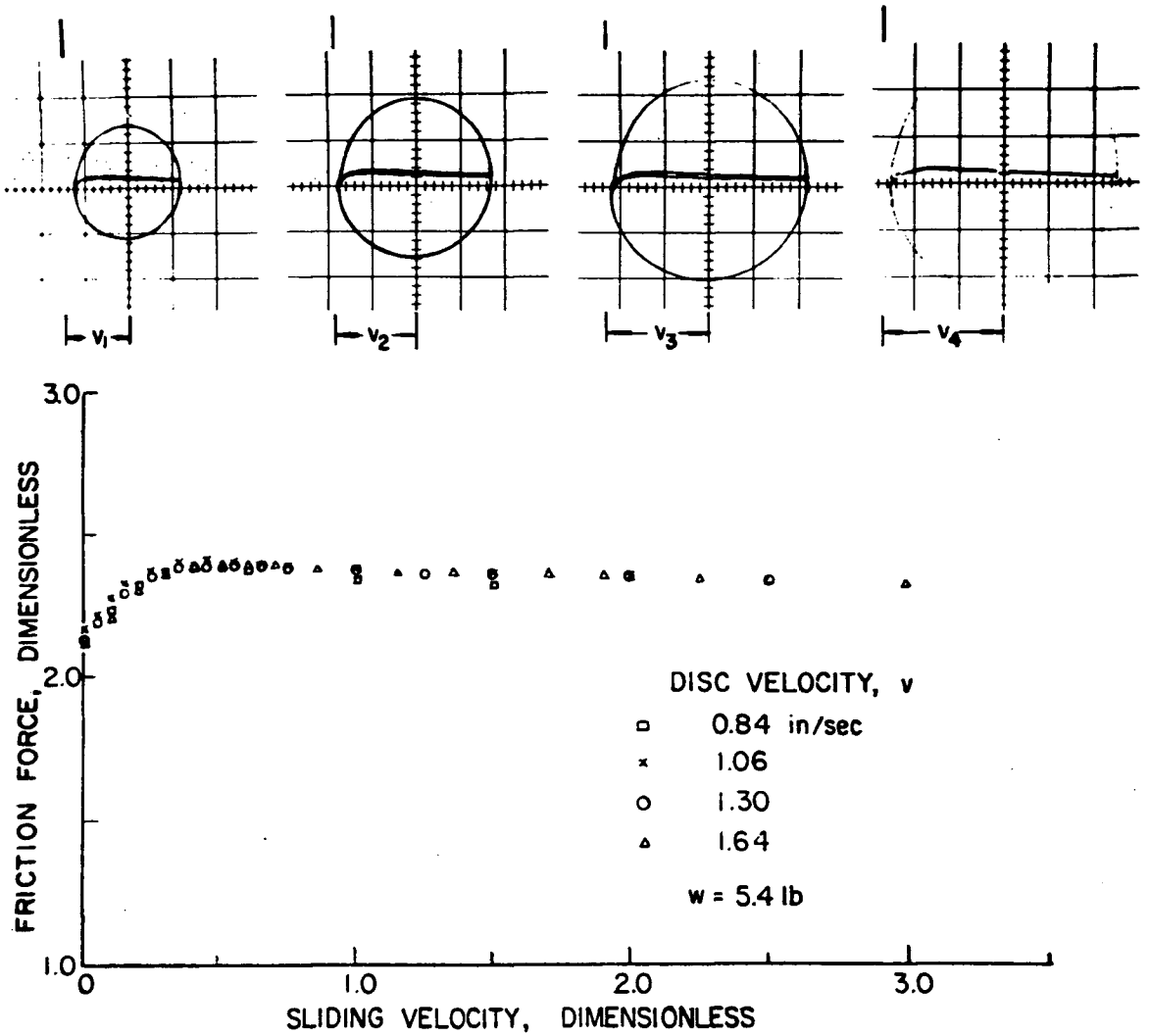

Figure 2.1.3 Kinetic Friction Force vs Velocity Relationship for Quasi-Harmonic Oscillation (Ko)

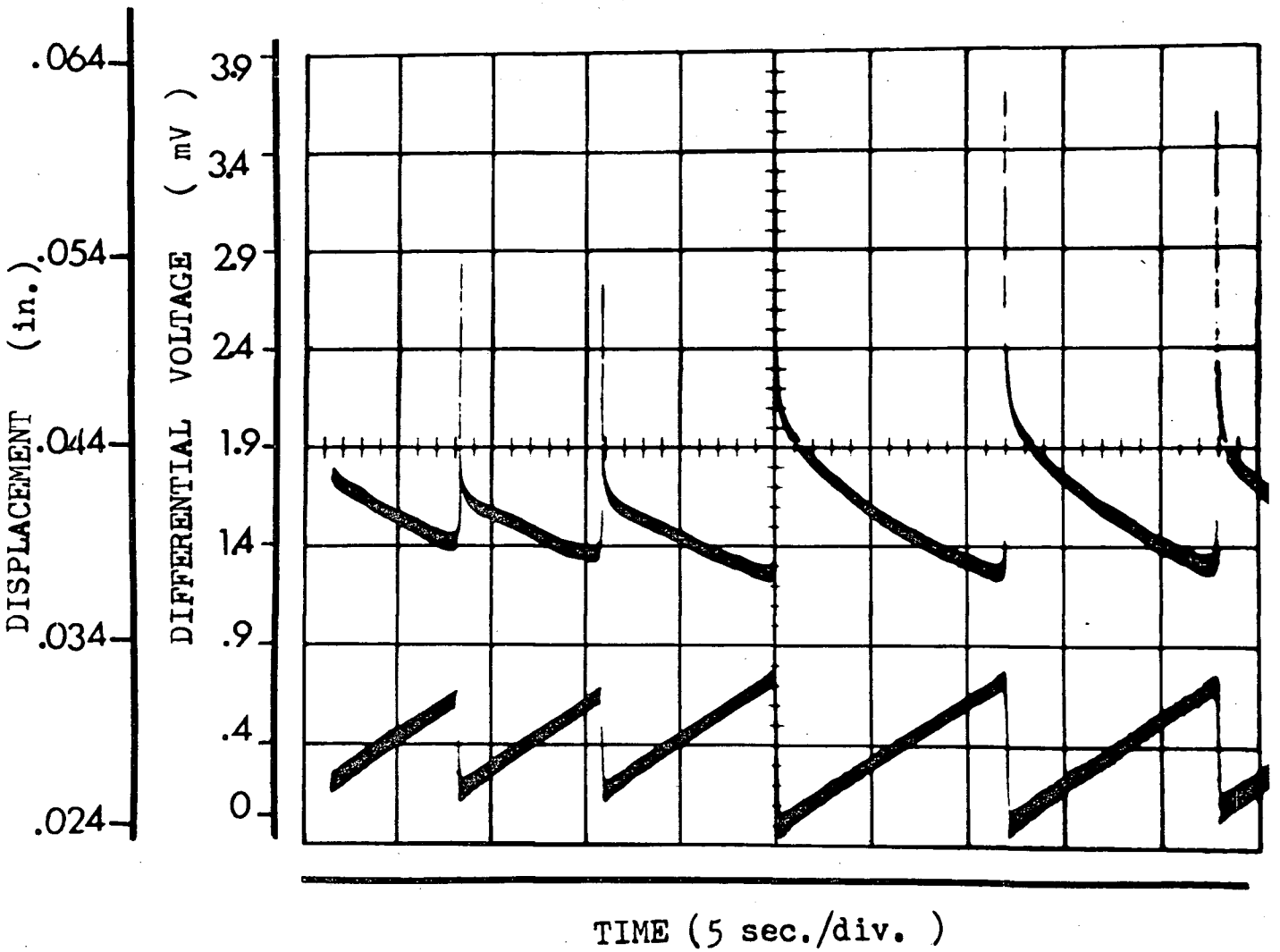

Figure 2.1.4 Interfacial Voltage Drop and Displacement Waveforms Recorded Simultaneously during Stick-Slip Oscillation (Green)

Upper Trace: Interfacial Voltage Drop
Lower Trace: Displacement

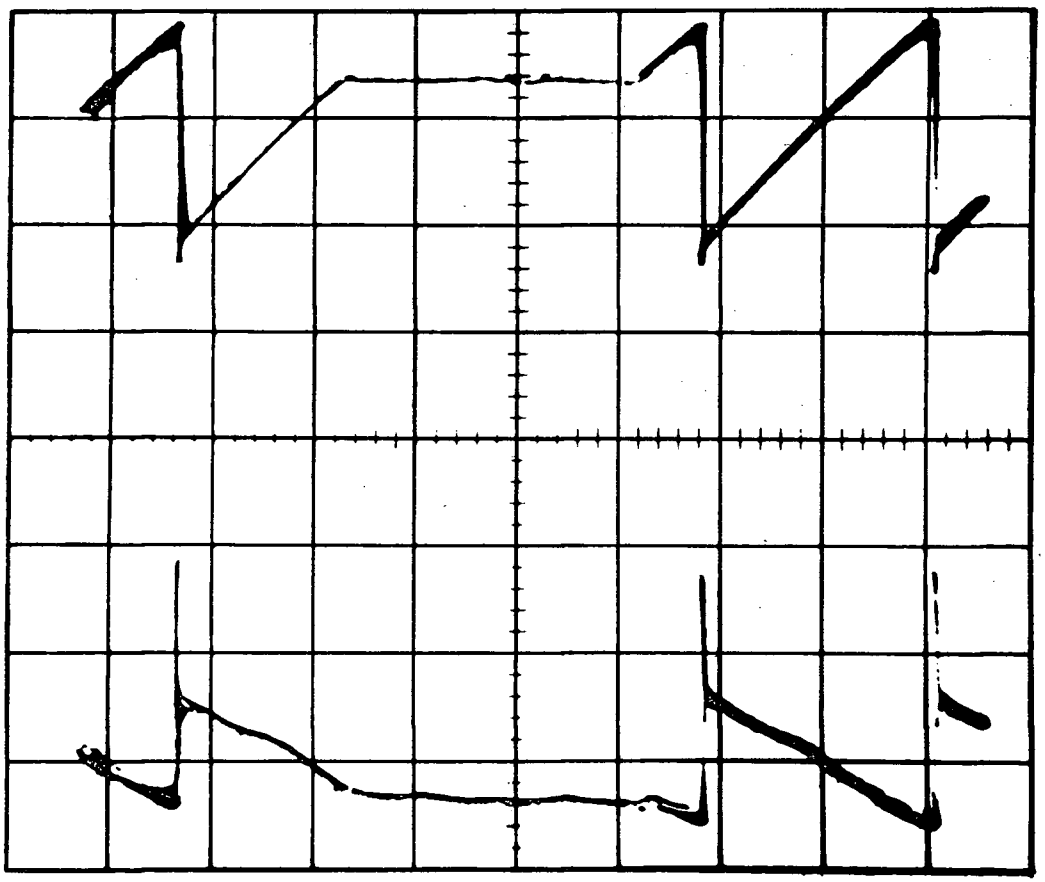

Figure 2.1.5 Effect on Interfacial Voltage Drop of Interrupted Tangential Load Application (Green)

Upper Trace: Tangential Load
Lower Trace: Interfacial Voltage Drop

CHAPTER III

III. THEORY

3.1 Static Friction

When two metallic surfaces are brought together under the influence of an applied normal load, they contact each other only at matching asperities (Fig. 3.1.1). Contact is initially elastic, but because the real area of contact is a very small portion of the apparent area of contact, the deforming metallic junctions might achieve a state of plasticity under minute loads, resulting in growth of the junction contact area until the real area of contact is just sufficient to support the applied load. Experimental evidence showing the area of contact to be directly proportional to applied perpendicular load was, for many years, thought to support this concept, proposed by Bowden and Tabor in 1950 [7]. Recently, however, certain investigators have presented analyses demonstrating that this proportionality of load and contact area might also be achieved under certain conditions of elastic contact. The most notable of these analyses was performed by Greenwood and Williamson [19], who showed that, for an exponential distribution of asperity heights, contact area could be proportional to load regardless of the mode of deformation. For most machined metal surfaces asperity heights have a near-Gaussian distribution; the Gaussian and

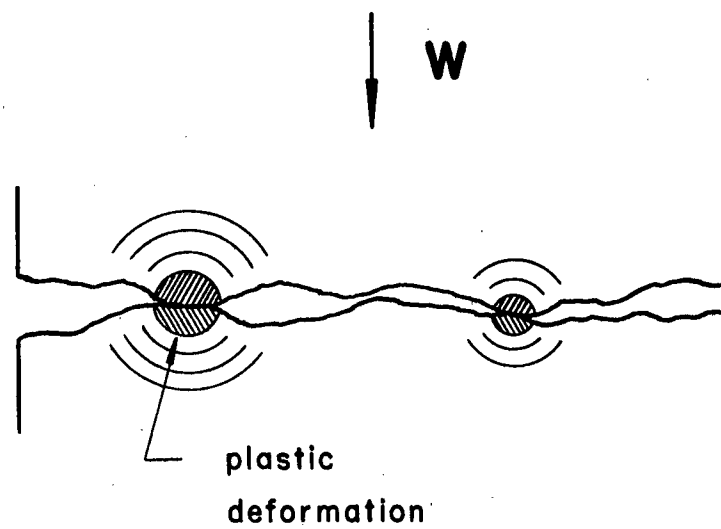

Figure 3.1.1 Nature of Metallic Contact at Interfacial Junction

Exponential distributions are sufficiently similar over most of the probability range to permit application of this study to conventional surfaces.

The first portion of the present investigation is devoted to an attempt to resolve the uncertainty concerning the mode of asperity deformation during static contact through development of a plausible plastic deformation model and comparison of its predicted behaviour with experimental static friction data.

Using Von Mises' yield criterion,

$$Y = \frac{1}{\sqrt{2}}\left[(S_1 - S_2)^2 + (S_2 - S_3)^2 + (S_3 - S_1)^2\right]^{\frac{1}{2}} , \qquad (3.1.1)$$

where S_1, S_2, and S_3 are the principal stresses and Y is the yield stress in uniaxial tension. For plane (two-dimensional) stress

$$Y^2 = S_1^2 + S_2^2 - S_1 S_2 , \qquad (3.1.2)$$

where

$$\left.\begin{matrix} S_1 \\ S_2 \end{matrix}\right] = \frac{\sigma_y}{2} \pm \sqrt{\left(\frac{\sigma_y}{2}\right)^2 + \tau_{yx}^2} \qquad (3.1.3)$$

in the co-ordinate system designated in Figure 3.1.2, and the yield criterion may be reduced to

$$Y^2 = \sigma_y^2 + 3\tau_{yx}^2 \quad . \qquad (3.1.4)$$

No analytic solution exists for a real three-dimensional contact, but empirical grounds exist [20,21] for alteration of equation 3.1.4 to

$$\sigma_0^2 = \sigma_y^2 + \alpha\tau_{yx}^2 \quad , \qquad (3.1.5)$$

where σ_0, the amount of compressive stress required to induce plastic yielding over the entire true area of contact in the absence of tangential stress, is approximately equal to 3Y [7]. Greenwood has shown [45] that α should have an approximate numerical value of 25 by the following reasoning.

If a metal, possessing a critical shear strength τ_0, can be assumed free of work-hardening, then

$$\tau_0 \cong \frac{1}{5}\sigma_0 \qquad (3.1.6)$$

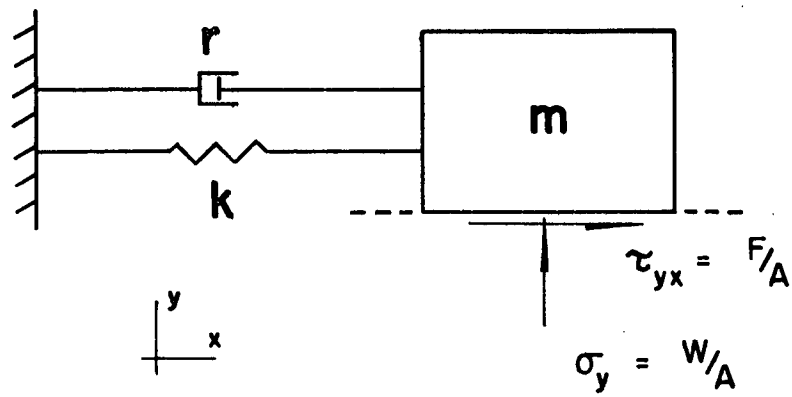

Figure 3.1.2 Co-ordinate System Adopted for Development of Area Growth Equation

for an axially symmetric contact [23]. Substitution in equation 3.1.5 yields

$$25\ \tau_0^2 \cong \sigma_y^2 + \alpha\tau_{yx}^2 \quad . \tag{3.1.7}$$

If, as is the case with clean metals in vacuum, the growth in the area of contact is very large, as a result of the tangential load τ_{yx}, then $\sigma_y << \tau_{yx} \cong \tau_0$, and $\alpha \cong 25$.

Attempts to measure α at the interface of two surfaces have resulted in values of $\alpha = 3.3$ for indium [20] and $\alpha = 12$ for platinum [9]. Errors inherent in the methods used for contact area measurement would result in conservative values of α, so that a numerical value of 25 does not seem unreasonable. So as not to be overly restrictive, α will be assumed to have a value between 10 and 25, a range of uncertainty which can be readily tolerated. As will be demonstrated, the present analysis is fortuitously insensitive to variation of this coefficient.

Substituting for σ_y and τ_{yx} in equation 3.1.5 yields

$$\sigma_0^2 = \left[\frac{W}{A}\right]^2 + \alpha\left[\frac{F}{A}\right]^2 \quad , \tag{3.1.8}$$

where A is the actual area of contact at the interface, F is the applied tangential load, and W is the normal load at the

interface; algebraic manipulation gives

$$\sigma_0 A = \left[W^2 + \alpha F^2\right]^{\frac{1}{2}} , \qquad (3.1.9)$$

a result derived by Tabor [22], provided the materials are in a state of equilibrium, a basic assumption of Von Mises' yield criterion.

In contacting asperities, where large shear strains develop in a relatively short period of time [9], a state of equilibrium cannot be supposed to exist. Anelasticity, or internal damping, of the materials must consequently be considered.

All solids display, in varying degree, the ability to dissipate vibrational energy [24]. The mechanical model most successfully used in the analysis of internal friction is the Poynting-Thomson model (Fig. 3.1.3), commonly called the "standard linear solid". For structural metals the contribution of k_2 to the behaviour of the model is negligible, except at rates of strain so great that the damper becomes a semi-rigid element. If such extreme rates are not achieved, the standard linear solid is effectively an elastic element (k_1) and an energy-dissipating element (r) acting in parallel, governed by the approximate equation

$$r\dot{\delta} + k_1\delta \cong P . \qquad (3.1.10)$$

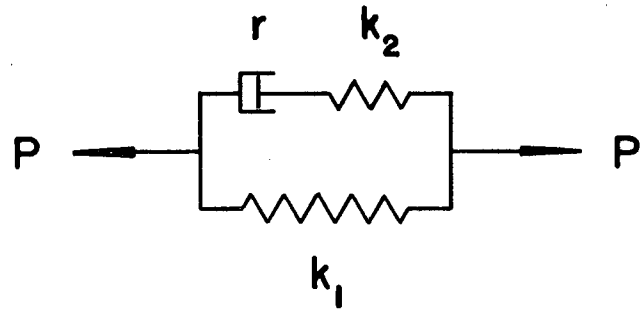

Figure 3.1.3 Poynting-Thomson Model for Analysis of Internal Frictional Dissipation

If the standard linear solid is in a state of equilibrium ($\dot{\delta} \cong 0$), its behaviour is entirely governed by the elastic element; if a state of equilibrium is not closely approximated, the contribution to equation 3.1.10 of the energy-dissipating element cannot be ignored.

The similarity of form of equations 3.1.9 and 3.1.10 for the condition of equilibrium ($\dot{\delta} \cong 0$) is obvious. If the analogy is to continue after altering equation 3.1.9 to include the effects of anelasticity, the modified equation must assume the form

$$r\dot{A} + \sigma_0 A = \left[W^2 + \alpha F^2\right]^{\frac{1}{2}} . \qquad (3.1.11)$$

Since dissipation is due to deformation of the metal, one might reasonably postulate that the amount of dissipation should increase with the volume of metal deformed. The area of contact, during indentation hardness tests, has been found to be proportional to the progress of a hemispherical elastic-plastic boundary within the test material, for all indenters except those with a very sharp apex [25]. The damping coefficient r may, therefore, be expressed as a power function of the area of contact.

$$r = r(A) = b A^n \qquad (3.1.12)$$

Substituting for r in equation 3.1.11 yields the proposed general equation of contact area growth under varying

tangential load,

$$b\,A^{n}\,\dot{A} \;+\; \sigma_0\,A \;=\; \left[W^2 + \alpha F^2\right]^{\frac{1}{2}} \quad . \tag{3.1.13}$$

Although equation 3.1.13 is of first-order form, no simple solution exists for the variation of the contact area A, as a function of time, under the influence of a ramp load $F = F_0 + \dot{F}t$, such as exists during the stick portion of a stick-slip cycle. Fortunately, the interest of this study is in the area of contact at the inception of slip, for which a general solution is not required.

The friction value at the inception of slip is the popularly-termed "static friction" coefficient μ_s. If gross sliding of the surfaces is deemed to occur as a result of the shearing of interfacial junctions, then

$$\mu_s \;=\; \frac{F_s}{W} \;=\; \frac{\tau_i A_s}{W} \quad , \tag{3.1.14}$$

where the subscript s designates values at the inception of slip, and τ_i is the ultimate shear strength of the interface.

Equations 3.1.13 and 3.1.14 form a pair of simultaneous differential equations. A_s, as given by equation 3.1.14, may be substituted into equation 3.1.13 to obtain

$$b\left[\frac{F_s}{\tau_i}\right]^{n} \dot{A}_s \;+\; \sigma_0\,\frac{F_s}{\tau_i} \;=\; \left[W^2 + \alpha F^2\right]^{\frac{1}{2}} \quad , \tag{3.1.15}$$

which may be algebraically manipulated to the form

$$\dot{A}_s = \left[\frac{\tau_i}{\mu_s}\right]^n \frac{W}{b}^{1-n} \left[\sqrt{1 + \alpha\mu_s^2} - \frac{\sigma_0}{\tau_i}\mu_s\right] \quad . \qquad (3.1.16)$$

As a consequence of entrapped contaminants, such as lubricant or oxide, the strength of the average interfacial junction formed by ideal plastic deformation of asperities may approach, but not equal, the shear strength of the metal substrate. Suppose, for example, that

$$\tau_i = K\,\tau_0 \quad , \qquad (3.1.17)$$

where K is a constant less than unity. As Tabor points out [22], if $\tau_{yx} = \tau_i$, $\alpha = 25$, and equation 3.1.7 is assumed to describe the limiting condition of stick, gross sliding will occur when

$$\frac{\tau_i}{\sigma_y} = \frac{1}{5(K^{-2} - 1)} \quad . \qquad (3.1.18)$$

Substitution into the standard equation for the coefficient of static friction yields

$$\mu_s = \frac{F_s}{W} = \frac{\tau_i\, A_s}{\sigma_y\, A_s} = \frac{1}{5(K^{-2} - 1)} \quad . \qquad (3.1.19)$$

Examination of equation 3.1.19 suggests that, if the interfacial shear strength equals that of the metal substrate, infinite

coefficients of static friction will be observed. Such is indeed the case with degassed metals at high temperature in high vacuum [26], where oxides and other contaminants are absent, if anelastic effects are minimized. However, the static friction coefficient, as determined by equation 3.1.19, falls to unity for a small reduction of K to 0.92, and to 0.5 if K is reduced to 0.85.

For normal frictional contacts there is consequently justification for assuming that the behaviour of the interfacial contacts is dominated by the properties of the metallic substrates. Specifically, the interfacial ultimate shear strength τ_i may be assumed to behave in a manner not unlike the substrates' ultimate shear strength, with respect to variation with strain rate.

Introduction of $\dot{\phi}$, the ratio of rate of tangential stress application divided by normal stress against which Johannes found that experimentally-determined values for the coefficient of static friction could be correlated, yields

$$\dot{\phi} = \frac{\dot{\tau}_{yx}}{\sigma_y} = \frac{1}{W}\frac{d}{dt}\left[\tau_i A_s\right] = \frac{A_s}{W}\dot{\tau}_i + \frac{\tau_i}{W}\dot{A}_s \quad . \tag{3.1.20}$$

If the term containing $\dot{\tau}_i$ is small in comparison to $\dot{\phi}$, a condition satisfied unless the interfacial shear strength τ_i exhibits strong rate dependence, equation 3.1.20 may be approximated by the relationship

$$\dot{\phi} = \frac{\tau_i}{W} \dot{A}_s \quad . \tag{3.1.21}$$

The validity of this approximation will be further discussed in section 5.1.

Substituting for $\dot{A}_s$ from equation 3.1.16 gives the result

$$\dot{\phi} = \frac{\tau_i^{1+n}}{W^n \, b \, \mu_s^n} \left[\sqrt{1 + \alpha \mu_s^2} - \frac{\sigma_0}{\tau_i} \mu_s \right] , \tag{3.1.22}$$

an equation describing the locus of μ_s, the coefficient of static friction, as a function of $\dot{\phi}$, the load rate variable. Examination of equation 3.1.22 will reveal that, as the load rate variable $\dot{\phi}$ approaches zero, the static friction coefficient μ_s must approach infinity, the interfacial shear strength τ_i must approach zero, or the parenthesized term must approach zero. In the presence of a lubricant μ_s cannot approach infinity. The interfacial shear stress τ_i may approach zero, due to metallic creep considerations, as $\dot{\phi}$ approaches zero, but certainly the two effects are not proportionate for any reasonable value of the superscript n; that is to say, $\dot{\phi}$ must be virtually zero before a substantial drop in τ_i from common values is observed [27]. The inescapable conclusion is that equation 3.1.22 can be satisfied for all $\dot{\phi}$, over

which stick-slip oscillation occurs, only if the parenthesized term equals zero at $\dot{\phi} = 0$. Therefore

$$\frac{\sigma_0}{\tau_i} = \left.\frac{\sqrt{1 + \alpha\mu_s^2}}{\mu_s}\right|_{\dot{\phi} = 0} = \left.\sqrt{\frac{1}{\mu_s^2} + \alpha}\right|_{\dot{\phi} = 0} . \qquad (3.1.23)$$

Both Von Mises' criterion and the less exact maximum-shear-stress theory show clearly that τ_0, the strength of the ductile substrate in pure shear, is proportional to σ_0. Since, for reasons already discussed, τ_i may be considered approximately proportional to τ_0, it logically follows that the ratio σ_0/τ_i will remain approximately constant, and independent of $\dot{\phi}$.

Use of this constancy permits rearrangement of equation 3.1.22 to the alternate form

$$\dot{\phi} = \frac{\sigma_0^{1+n}}{W^n b \mu_s^n \left[\frac{\sigma_0}{\tau_i}\right]^{1+n}} \left[\sqrt{1 + \alpha\mu_s^2} - \frac{\sigma_0}{\tau_i}\mu_s\right] . \qquad (3.1.24)$$

Consideration of the nature of the substrate tensile strength σ_0, at the inception of slip, remains.

The simplest solution of equation 3.1.24 results from assuming σ_0 and, therefore, τ_i, to be a constant. As data from Nadai and Majoine [27], presented in Figure 3.1.4, shows,

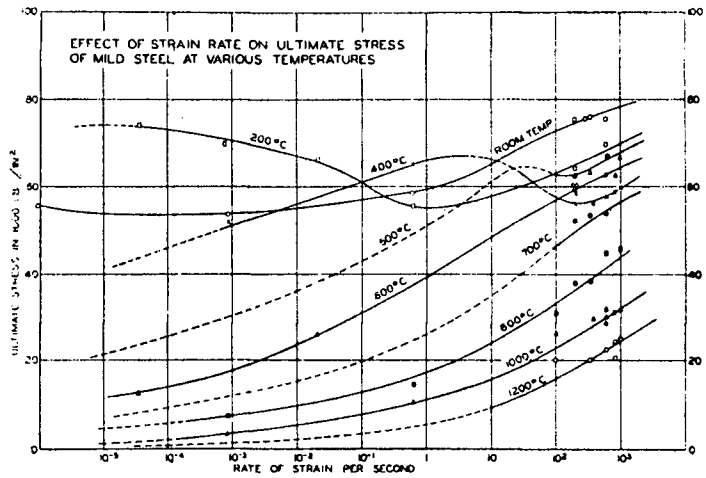

EFFECT OF STRAIN RATE ON ULTIMATE STRESS OF MILD STEEL AT VARIOUS TEMPERATURES

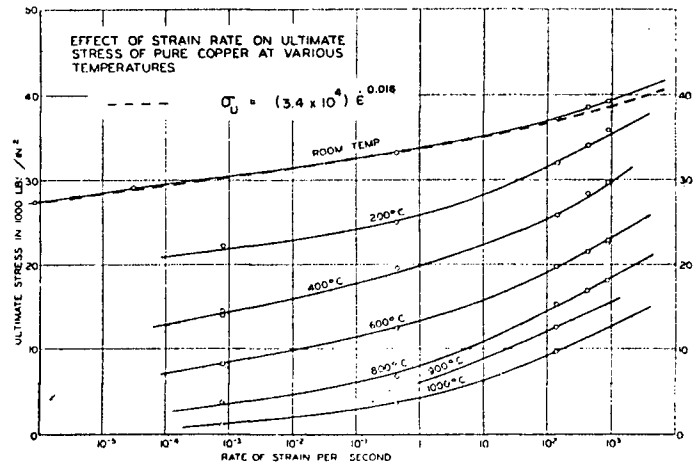

EFFECT OF STRAIN RATE ON ULTIMATE STRESS OF PURE COPPER AT VARIOUS TEMPERATURES

Figure 3.1.4 Effect of Strain Rate on Ultimate Tensile Strength of Mild Steel and Copper (Nadai and Majoine)

this condition of constancy is approximately satisfied, over a large range of strain rate, by mild steel at room temperature. Most metals, unfortunately, have less convenient behaviour. Copper, for example, at room temperature appears to follow a relationship of the form

$$\sigma_0 = K \dot{\varepsilon}^m \qquad (3.1.25)$$

at fracture. Brass, whose lattice structure is unchanged from that of copper by the addition of zinc, and whose major component is copper, might be expected to also exhibit behaviour described by equation 3.1.25. Consideration of the effect of rate dependence of σ_0 on equation 3.1.24 will be deferred until section 5.1, where individual frictional examples are discussed.

3.2 Kinetic Boundary Friction

Section 3.1 was devoted to original development of an equation predicting the variation in the static friction coefficient with rate of loading. In contrast, this section will be concerned with the basic concepts required for the discussion of kinetic results from the present study.

The simplest form of friction, under steady-state conditions of sliding, consists of a retardation force, totally independent of relative velocity between surfaces, called Coulombic friction. An example of a Coulombic friction force trace on the phase plane, together with a generated behavioural trace for a spring-mass system, subject to this friction force in free vibration, may be found in Figure 3.2.1. Coulombic friction is approximated in many instances of nominally unlubricated contact of harder metals [28,29]. The expression "nominally unlubricated", rather than "unlubricated", is used because crude lubrication is inherent in the presence of most metallic oxides.

Contrary to its proven minimal effect on the governing mechanism of static friction [9], in which its sole function appears to be the decreasing of the interfacial shear strength, the presence of a liquid lubricant, even without chemical boundary lubrication additives, may have a profound effect on the observed frictional behaviour under kinetic conditions. These chemical additives are normally long-chain polar molecules, which attach by one end to the metal surface, or

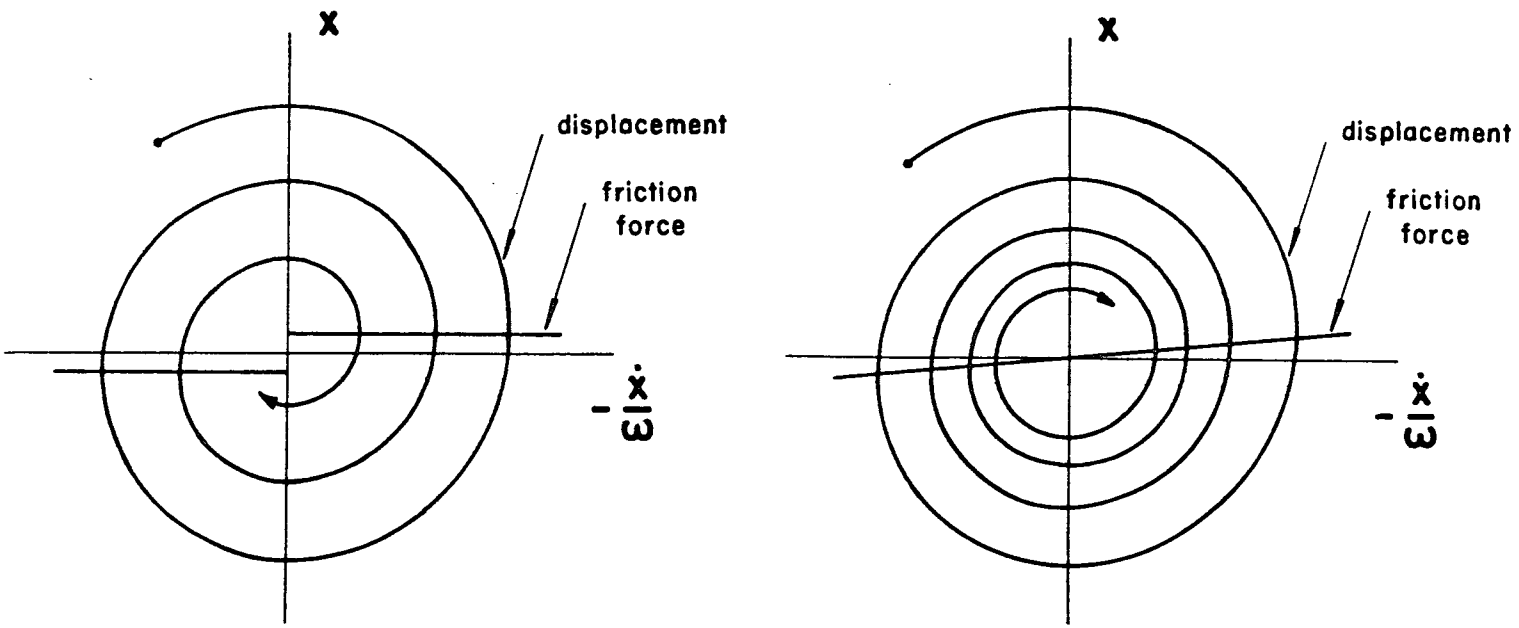

Coulombic Friction

Linear Viscous Friction

Figure 3.2.1 Free Vibration of a Linear Spring-Mass System Subject to Simple Forms of Friction

compounds (organic or inorganic) which react with metallic oxides to form a film of low shear strength. Chemical additives which do not appreciably affect the lubricant viscosity have no effect on frictional behaviour until opposing surfaces are sufficiently close that the thickness of an additive layer is a substantial portion of the gap between surfaces. If the surfaces do not achieve such close proximity, or if chemical action between the lubricant and surfaces is negligible, frictional behaviour is governed by the viscous properties of the lubricant.

Linear viscous friction is a simple form of energy dissipation associated with the presence of a Newtonian fluid between two parallel, plane surfaces. A Newtonian fluid is a viscous fluid in which the rate of shear is directly proportional to the applied shear stress, as expressed by the equation

$$\tau_{yx} = \eta \frac{du}{dy} \quad . \tag{3.2.1}$$

If two plane surfaces are separated by a Newtonian fluid layer of constant thickness, the variation in tangential friction force with relative velocity of the surfaces is linear. Figure 3.2.1 shows an example of linearly viscous dissipation action, together with a generated free vibration behavioural trace, on the phase plane.

Another important effect associated with fluid viscosity

is that of a squeeze film. As examination of Appendix III will reveal, a plane surface with a circular periphery, which approaches another, parallel plane surface from which it is separated by a Newtonian liquid of invariant viscosity, has a load-bearing capacity

$$N_f = -\frac{3}{2}\pi\eta R^4 \cdot \frac{1}{h^3}\frac{dh}{dt} \quad , \tag{3.2.2}$$

where h is the gap between surfaces. The rate of change of the surface gap, $\frac{dh}{dt}$, is very small, for any normal load N_f, if the surface separation is small. Note particularly that equation 3.2.2, derived for the case of parallel surfaces, is applicable whether or not relative motion, and a consequent viscous tangential retardation force, exists between the surfaces in their own plane.

Full hydrodynamic lubrication results from the pumping of a viscous fluid through a converging gap between solid surfaces. These solid surfaces do not touch, and fluid pressures are usually sufficiently low that surface profiles remain essentially unaltered. Observed frictional resistance to motion of one surface tangential to the other is a consequence of the energy expended in overcoming viscous drag. Hydrodynamic analysis traditionally considers bearing surfaces smooth, requiring that they be non-parallel in order to generate load-carrying pressures in the lubricant. However,

the generation of hydrodynamic lift between closely-spaced parallel surfaces is well documented, if not well understood [30]. Explanations advanced for this phenomenon have included thermal expansion of the lubricant, thermal deformation of the surfaces, and hydrodynamic lift, on a microscopic scale, as a consequence of surface rugosity.

If hydrodynamic lift is to occur as a consequence of surface rugosity localized load-carrying pressures may be very much greater than the mean liquid pressure between the surfaces. The rigidity of surfaces normally assumed in hydrodynamic analysis becomes a questionable supposition. Of definite interest, then, is the field of study called elastohydrodyanmic lubrication. Elastohydrodynamic lubrication analysis was developed because of the inadequacy of classical hydrodynamic analysis to explain the occurrence of effective hydrodynamic lubrication in extreme-pressure point and line contacts, the transmission of forces between gear teeth being one example. Elastohydrodynamic theory is distinguished from classical hydrodynamics by specification of the lubricant film thickness as a function of the elastic properties of the load-bearing solid surfaces, as well as of the applied load, lubricant viscosity, and initial surface geometry. Elastohydrodynamic theory, in its simplest form, requires simultaneous solution of equations of hydrodynamics and elasticity.

Exact analytic solutions are not usually achieved for even the simplest cases of elastohydrodynamic lubrication.

Consider, therefore, the increased difficulty of solution as changes in lubricant viscosity due to pressure, temperature, and shear rate sensitivity are included in the equations. Numerical techniques, utilizing digital computer facilities, are normally employed. One of these numerical solutions, verified experimentally [31], for the very simple case of two cylindrical rollers with identical surface velocities in the contact zone, is displayed in Figure 3.2.2, together with comparable solutions for purely elastic and classical hydrodynamic cases.

The elastohydrodynamic lubrication property that is of special interest to the present study is the generation of friction forces when the opposing surfaces possess a non-zero tangential relative velocity. A family of experimentally-obtained curves, displaying the variation of friction force with relative velocity of the surfaces for the case of parallel cylindrical rollers, is presented in Figure 3.2.3. The lubricant employed was a commercial mineral turbine oil, British Admiralty specification OM 100, and the rollers were hardened steel, diameter 3 inches. The initial rise in friction force with relative velocity is consistent with the properties of an isoviscous Newtonian lubricant; but as relative velocity increases, friction forces become increasingly less than those predicted from isoviscous considerations, to the extent that measured friction force decreases with increasing relative velocity at high relative velocity values.

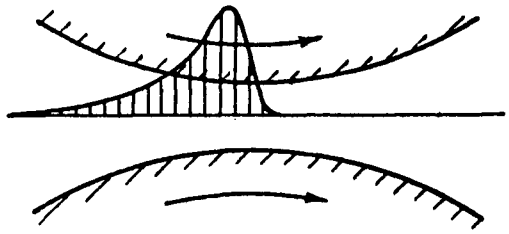

Martin conditions—rigid solids, isoviscous lubricant

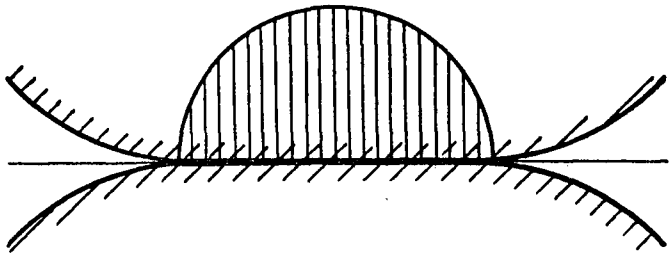

Hertzian conditions—dry contact, elastic solids.

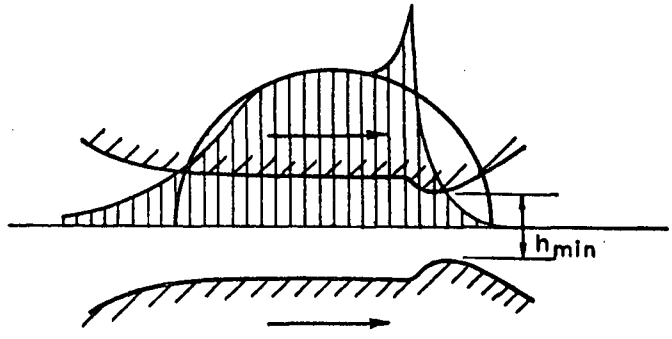

Elastohydrodynamic conditions—elastic solids, Newtonian lubricant

Figure 3.2.2 Rolling Contact Conditions [42]

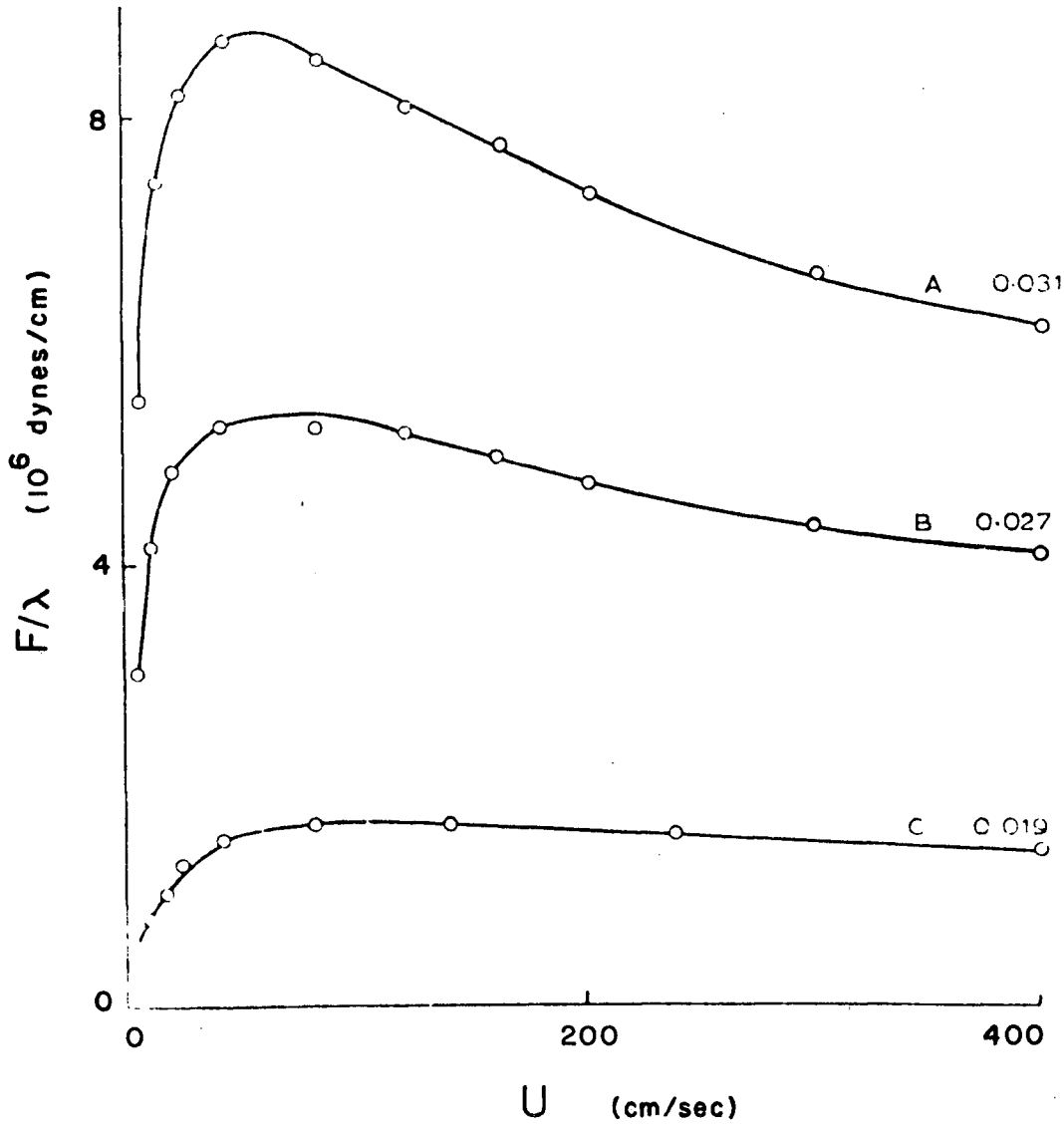

Figure 3.2.3 Elastohydrodynamic Friction Force vs Velocity Curves [43]

U = 400 cm/sec. Normal loads (10^6 dynes/cm)-- A:20, B:15, C:7.5. Values of μ at U = 400 cm/sec shown at right of curves

Experts in the field credit this reduction in friction force to viscosity decreases resulting from thermal effects of viscously-generated heat.

Crook [32] has developed, in explaining the curves of Figure 3.2.3, an approximate relationship of the form

$$\frac{F}{\lambda} = \frac{\bar{\eta}\, U\, \Delta}{h_{min}} \quad , \tag{3.2.3}$$

Δ = length of rectangular load-carrying film

λ = width of rectangular load-carrying film

$\bar{\eta}$ = mean effective liquid viscosity

h_{min} = minimum film thickness (Fig. 3.2.2)

in which the mean effective liquid viscosity is itself expressed by an approximate heat-transfer relationship

$$\bar{\eta} = \frac{\xi_f}{\gamma\, U^2}\left[\frac{\psi W}{\lambda \Delta} + 2 \ln U + \ln \frac{\eta_s \gamma}{2\xi_f}\right] \quad , \tag{3.2.4}$$

ξ_f = thermal conductivity of lubricant

η_s = lubricant viscosity at temperature of bounding friction surfaces

$\gamma = \frac{1}{T - T_o} \ln \frac{\eta_o}{\eta}$ = coefficient of lubricant viscosity variation with temperature

$\psi = \frac{1}{p - p_o} \ln \frac{\eta}{\eta_o}$ = coefficient of lubricant viscosity variation with pressure.

In standard elastohydrodynamic situations h_{min} is a function of mean surface speed, lubricant properties, and load. If, however, for boundary lubrication situations a nearly constant, substantial portion of the normal load is demonstrably supported by asperity contact, h_{min} is, for practical purposes, approximately constant. Asperity contact does not mean that h_{min} necessarily assumes the value zero, as equation 3.2.3 might suggest. That equation, derived from a two-dimensional model, makes no allowance for lateral flow of lubricant, which must occur at any point of contact between the surfaces. When attempting to apply equation 3.2.3 to such circumstances the variable h_{min} can no longer be interpreted as true minimum clearance; it must instead assume some effective positive value determined by summation of elastohydrodynamic effects over the total load-bearing film.

During this study the load and load-bearing film area and shape were unaltered. If, as additional conditions, one assumes h_{min} and η_s constant, Crook's frictional relationships may be reduced to the form

$$F = \frac{a}{U}\left[b + \ln U \right] , \qquad (3.2.5)$$

which will exhibit a maximum at some value of relative velocity determined by the constant b. This maximum is relevant to discussion of quasi-harmonic oscillation, which will follow in section 5.2.

Having reviewed the foregoing concepts of lubricated kinetic friction, it is apparent that even a chemically inert liquid lubricant can contribute to or dominate the boundary friction behaviour of metallic surfaces by purely viscous action. The effects of chemical action between lubricant and surfaces add to the effects of viscous action, making analysis of a complex situation even more involved. Chemical effects have consequently, as much as possible, been eliminated from the present investigation so as to permit a more certain analysis of the physical friction mechanisms involved.

CHAPTER IV

IV. APPARATUS AND EXPERIMENTAL PROCEDURE

4.1 Apparatus

Because a certain portion of relatively high-speed investigation was anticipated, the use of a linear-motion friction apparatus, of inherently limited track length, was discarded in favour of a rotary-motion apparatus, in which the track length can be made effectively infinite. The apparatus used by Ko [15], which required minimal modification to suit it for the present study, was utilized. A schematic diagram of this apparatus, as employed, may be found in Figure 4.1.1.

The friction couple consisted of a rotating steel disc, of diameter 4 inches, on which rested a slider of diameter 3/8 inch. The slider was pressed into a hemispherical mount, which provided a means of initial alignment of the slider with the disc surface. Load application and elastic restraint of the slider were provided by a compound cantilever beam passing across the disc, in order that the curvature of the slider path was in the same sense as that of the friction track on the disc. Applying load, as well as restraint, by means of the beam permitted independent variation of load and the frequency of free vibration of the system. A compound, rather than simple, beam was used

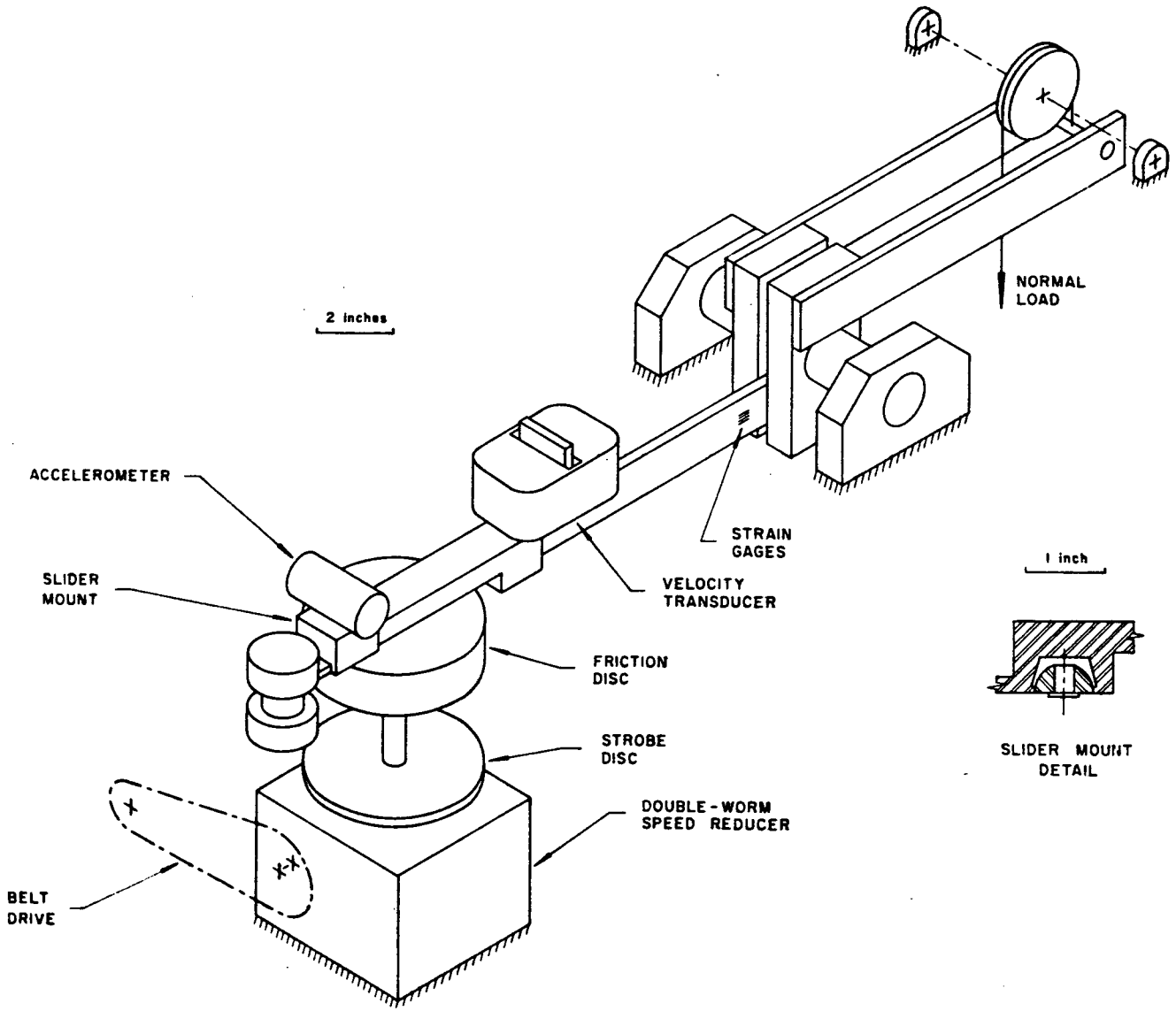

Figure 4.1.1 Schematic Diagram of Experimental System

in order that force application could be at the projected neutral axis of the more elastic portion of the beam, eliminating undesirable torsional effects in the beam due to friction forces at the interface. To minimize torsional effects due to dynamic imbalance, lead weights were attached to the end of the beam in such a fashion as to also place the center of gravity of the vibrating mass on the fore-mentioned neutral axis.

The "fixed" end of the cantilever beam was clamped to a rigid steel shaft mounted in self-aligning pillow-block bearings. These bearings were end-loaded to eliminate slack, and mounted firmly to an aluminum shell. This shell, and the base on which it rested, were both heavily weighted with lead, so as to reduce, as much as possible, the natural frequency of vibration of the friction mechanism's supporting structure. This reduction in the supporting structure's natural frequency isolated the friction mechanism from external vibration to which it would be most sensitive by locating these "noise" frequencies well into the strongly-attenuated portion of the structure's transmissibility spectrum. Such precautions were exercised because several investigators, the most notable among them being Fridman and Levesque [33], have found that the application of external frequencies to a friction surface substantially decreases the observed values of static friction.

The drive train utilized a 100:1 double-worm speed reducer immediately preceding the driven steel disc. This reducer, as a result of its sequential double-worm construction, negated the transmission of torque variations, at the friction surface, back to its power input shaft. That this input shaft exhibited a non-fluctuating reaction torque was essential to obtaining a uniform driven-surface velocity, since the remainder of the power transmission system consisted of jointless, soft rubber O-rings.

The elasticity of these O-rings (manufactured for use as seals) made a direct, motor-to-disc, belt type of power transmission system impractical. Unfortunately, more common modes of power transmission were even more impractical. Spur gears generate vibration as a consequence of the meshing of teeth; conventional drive belts have joints, which generate force impulses when passing over drive pulleys. A drive train consisting solely of worm reducers would generate little noise, but would be both clumsy and costly, as well as providing an excellent noise path from the motor to the friction surface. The hybrid system, O-rings driving a worm reducer, which provided uniform surface speeds, good noise isolation, and extreme flexibility, was employed very successfully.

The O-ring portion of the drive train was, in reality, a dual system. One portion of this system consisted simply of a variable-speed 3/16 hp. d.c. motor directly driving the worm reducer through a single O-ring. This part

of the system, though not strictly necessary, was convenient for the production of the higher surface speeds employed in this investigation. The other portion of the dual system consisted of a 1 hp. variable-speed d.c. motor driving the worm reducer through a noise-free, multi-ratio speed reducer, constructed of O-rings and pulleys, possessing a maximum reduction capability of 10^4.

Surface speeds at the friction track radius ranged from 3×10^{-5} in/sec. to 12 in/sec. Higher speeds could have been readily achieved, but were not required. Photographs of the system may be found in Figures 4.1.2 and 4.1.3. System parameters may be found in Appendix I.

4.2 Measurement of Friction Forces

Measurement of friction forces between the slider and the disc was required under dynamic conditions, when the slider and beam would be subject to non-negligible acceleration forces. Simple measurement of beam displacement, a procedure commonly employed in the past for both static and dynamic investigations, would have been inadequate for obtaining such information because it ignores these important inertial forces. The electrical summation methods of Bell and Burdekin [12] were consequently employed.

The equation of motion of the slider may be written in the form

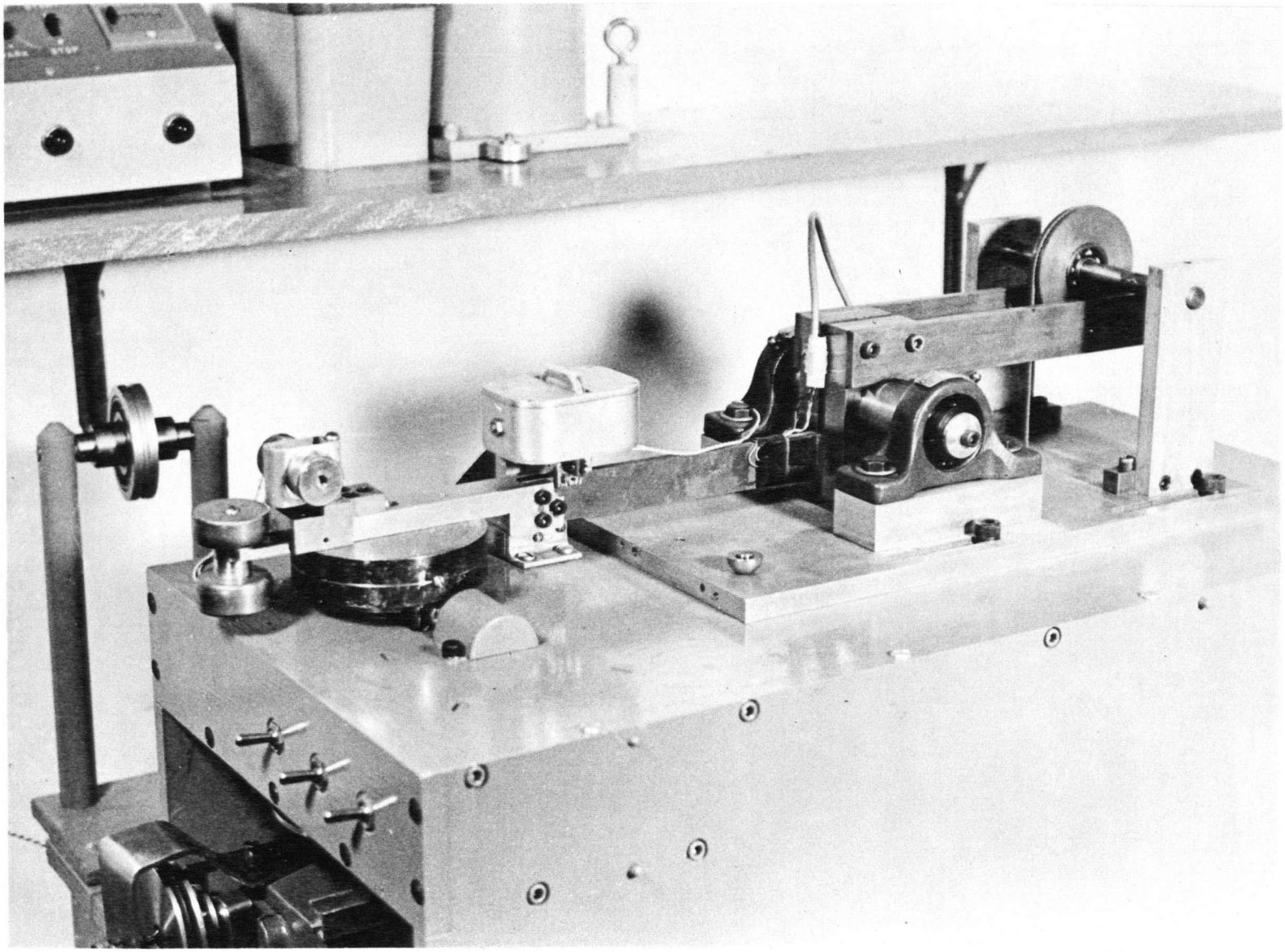

Figure 4.1.2 Vibratory System, with Instrumentation

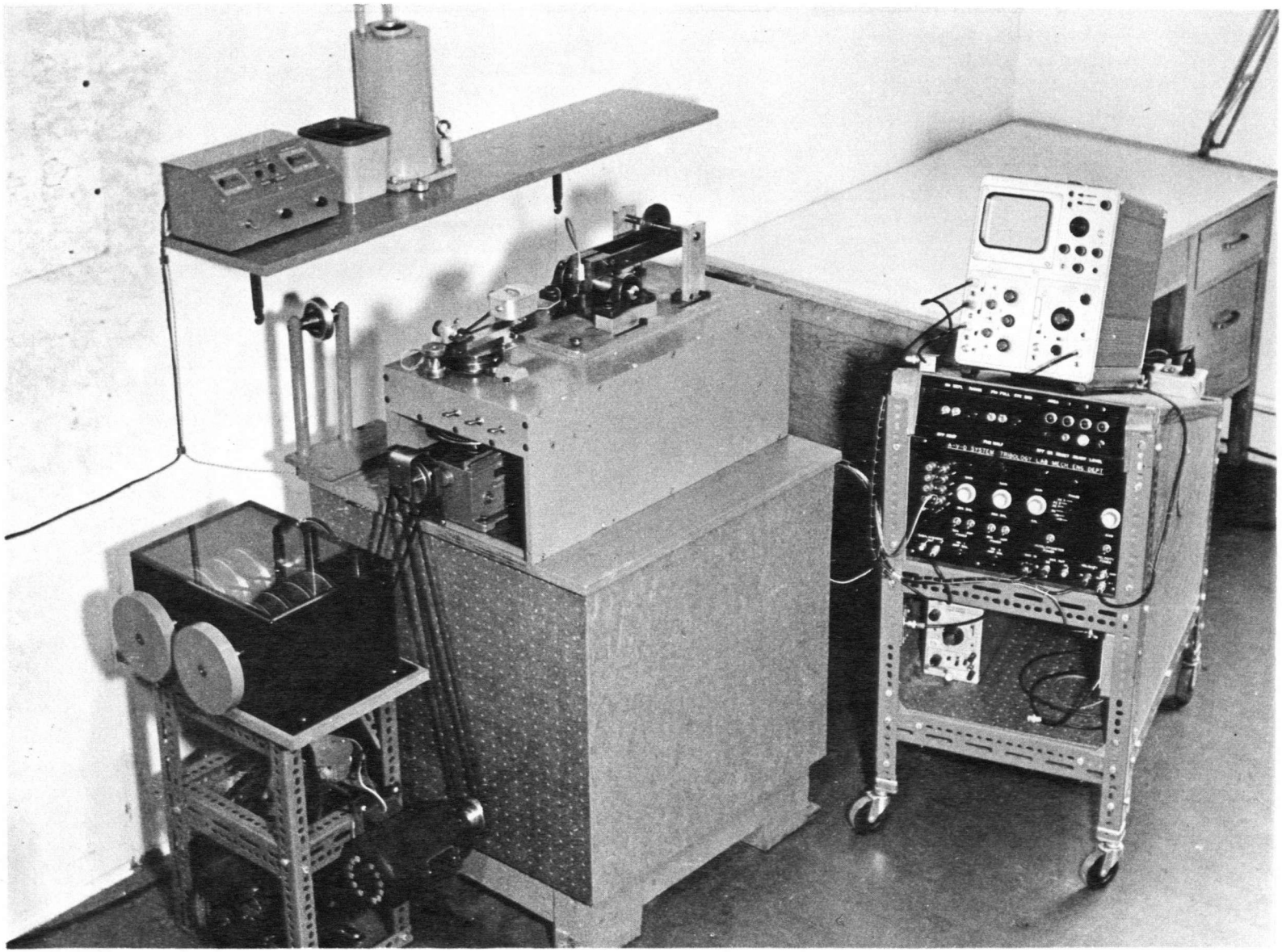

Figure 4.1.3 Complete Experimental Apparatus

$$M\ddot{x} + r\dot{x} + k\,x = F \quad , \tag{4.2.1}$$

where M is the equivalent mass of the slider and its supporting structure, and F is the friction force experienced by the slider at its interfacial surface. Rearranging this equation to the form

$$\ddot{x} + \frac{r}{M}\dot{x} + \frac{k}{M}x = \frac{1}{M}F \tag{4.2.2}$$

plainly illustrates that, if the viscous dissipation term $\frac{r}{M}\dot{x}$ is of negligible magnitude, with respect to the other terms, a scaled measure of the friction force may be obtained from the summation of the slider acceleration and the displacement signals, properly scaled.

Examination of Appendix I will confirm that $\frac{r}{M}$ is four orders of magnitude smaller than $\frac{k}{M}$. From phase plane analysis, and the knowledge that motion of the slider with respect to the friction surface is performed under energy-dissipating conditions, maximum velocity $\dot{x}_{max}$ is less than the maximum displacement x_{max} multiplied by the natural frequency of vibration of the slider and its supporting structure, ω_n (Appendix II). The damping term is therefore two orders of magnitude less than the displacement term, with respect to their individual maxima, and may consequently be assumed to make a negligible contribution to the equation

of motion, permitting equation 4.2.2 to be rewritten in the form

$$\ddot{x} + \frac{k}{M} x = \frac{1}{M} F \quad . \qquad (4.2.3)$$

Vectorial summation of the acceleration and displacement was achieved by transmitting the two signals to the oscilloscope differential amplifier.

The accuracy of all friction measurements was restricted to that of the principal data recording instrument, an oscilloscope. A more precise recording device would have been of no advantage because the instrument signals exhibited a superimposed high-frequency mechanical noise component, most prominent on the acceleration signal and least prominent on the displacement signal. The noise signals were most pronounced during quasi-harmonic oscillation and following the inception of slip. Possible explanations for this unwanted noise generation include vibration of portions of the cantilever beam's support structure and vibration of the beam in non-fundamental modes.

4.3 Instrumentation

a. Displacement

Two 350 ohm strain gages were mounted at the root of the cantilever beam, where bending moments in the beam were at a maximum. These gages, together with two identical gages

used for temperature compensation purposes, were employed in a four-arm bridge circuit. Bridge output was amplified by an electronic unit similar to Ellis Associates' Bridge Amplifier Meter, model BAM-1.

b. Velocity

An electromagnetic transducer, consisting of a coil of enamelled wire positioned in a constant magnetic field, was situated such that, during beam vibration, the conductors moved transversely to the direction of the fixed magnetic field. Generated voltage was consequently proportional to the instantaneous velocity of the coil. This voltage signal was attenuated by a variable-output voltage divider circuit before transmission to the recording instruments. Details of the transducer may be found in Figure 4.3.1.

c. Acceleration

A self-contained servo accelerometer, Kistler model 305A, was mounted on the specimen holder. Direct transmission of the acceleration signal to the recording instruments was possible because a 30 volt d.c. power source yielded a maximum accelerometer voltage of ±5 volts. The level of acceleration corresponding to maximum signal, which could be altered by changing an external resistor, was set at 50 g, yielding a sensitivity of 0.1 volt/g. Maximum resolution of the instrument was better than 5×10^{-7} volts, or 5×10^{-6} g.

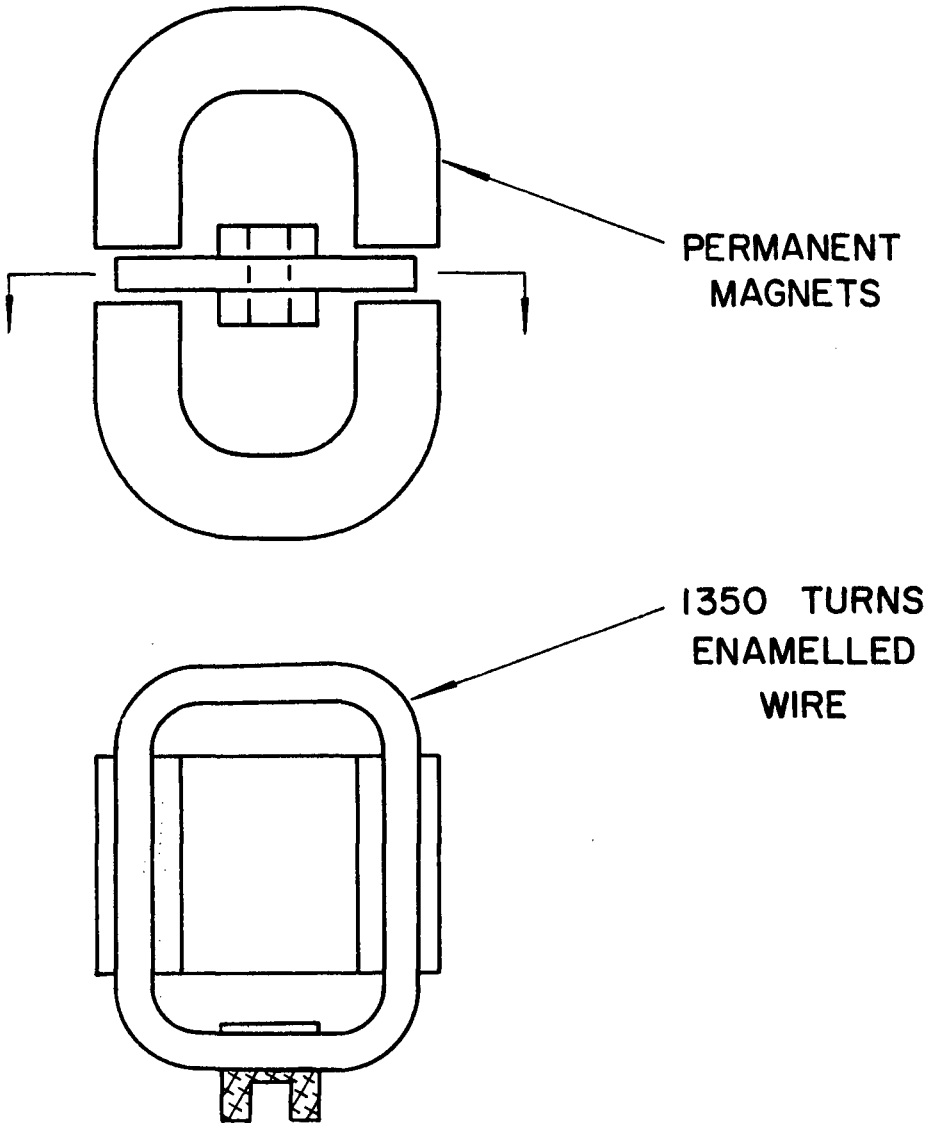

Figure 4.3.1 Velocity Transducer Detail

d. Recording Instruments

Instruments used for recording data were a Brush dual channel rectilinear oscillograph, Mark 842, and a Tektronix dual beam storage oscilloscope, Model 564. The oscilloscope was equipped with a dual-beam differential amplifier, Type 3A3, a single-beam differential amplifier, Type 2A63, and a time-base amplifier, Type 2B67. The single-beam differential amplifier and the time-base amplifier were used interchangeably. The oscilloscope was modified so as to permit control of its beam-blanking circuit by an external voltage signal.

e. One-Cycle Sequential-Triggering Circuit

Control of the oscilloscope's beam-blanking circuit was performed by an external circuit, similar in function to that used by Ko [15], constructed to permit the recording of a single cycle of vibration. This circuit was, in turn, controlled by the displacement signal.

The one-cycle circuit, which may be found in Figure 4.3.2, essentially consisted of three relays surrounded by accessory circuitry. The first and third relays were tripped by a given level of negative displacement signal to, respectively, unblank and reblank the oscilloscope beam. The second relay, tripped by a preset positive displacement signal level, served as an interlock, preventing "machine-gunning" of the first and third relays on the same negative displace-

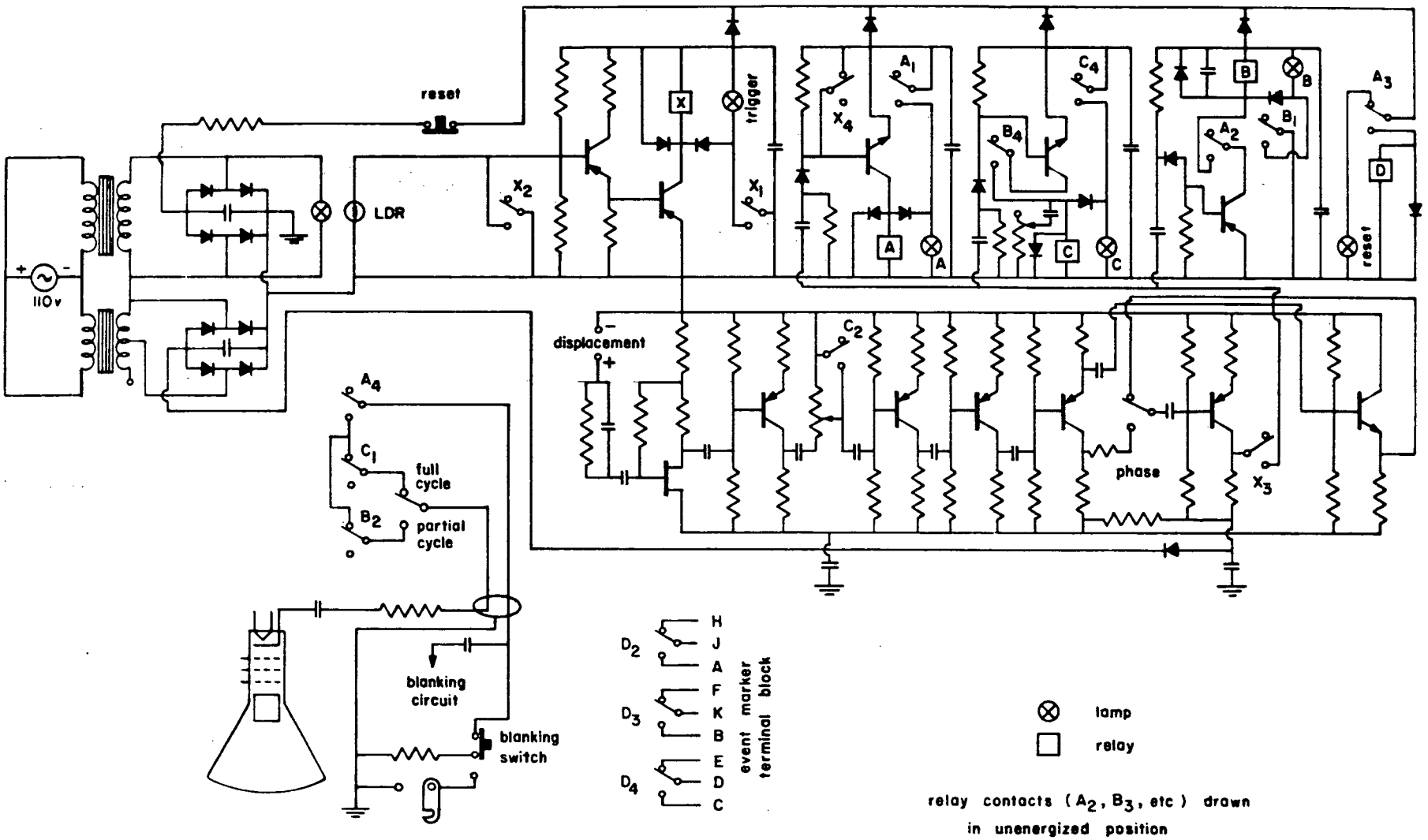

Figure 4.3.2 Spot-Triggering and Sequential-Triggering Circuitry

ment signal. This trio of relays was energized by a key relay; all four relays were simultaneously reset by a manually-transmitted voltage signal.

f. Spot Triggering

To minimize inconsistency of results due to possible non-uniformity of the driven disc's surface, recorded data, throughout the duration of a test, was obtained from a very restricted portion of the disc's friction track. A light-discriminating resistor (LDR) was used to signal the key relay, in the one-cycle sequential-triggering circuit, of the arrival of this predetermined portion of the friction track at the slider's location. Details of the spot-triggering circuitry are included as an integral part of the sequential-triggering circuit presented in Figure 4.3.2. Each time a flag, which could be fixed at any desired point on the disc's circumference, moved between a light source and the LDR a voltage pulse was transmitted to the key relay. If the relays had been previously reset the key relay would activate the blanking-circuit control relays, resulting in the recording of information over the duration of the succeeding cycle.

The advantage of using a LDR triggering system, rather than a simpler, mechanical trigger, lay in the fact that no triggering-force reactions were experienced by the drive train. Mechanical devices, even those as effortless in operation as microswitches, had switching reactions which appeared as non-negligible acceleration signals. Any such

acceleration spike could initiate slip, if the friction surfaces were approaching the limiting conditions of stick, and/or have a transient effect of sufficient duration to affect the recorded data.

g. Speed Determination

Belt stretch, and possible belt slippage, rendered indirect measurement of friction disc speed, at some remote portion of the drivetrain, totally unfeasible. The reasons negating use of a mechanical spot-triggering device made employment of a mechanically-driven speed indicator equally unwise. A displacement indicating device, consisting of a precisely-machined strobe disc separating a light source and a LDR, was consequently constructed. The strobe disc was mounted on the shaft driving the friction disc, and the light source-LDR combination fixed to the apparatus frame. Signals from the LDR were registered by a counter operating in conjunction with an elapsed-time indicator. Error in speed determination, greatest at higher speeds, was less than $\pm 2\%$.

4.4 Specimens

As a consequence of the work of Davis [13], the testing of a range of different metals was deemed unnecessary. The initial intention was, therefore, to test only one friction pair. A steel-on-steel friction couple was chosen. But when

unique and interesting results were obtained, outside the range of load rate encompassed by Davis' experiments, it became prudent to confirm the similarity of action of different metals over this extended range, so as to avoid the possibility of drawing general conclusions from anomalous behaviour. Confirmatory tests were performed using unleaded brass sliding on steel, another common industrial pair.

The 3/8 inch diameter sliders and the 4 inch diameter steel disc, whose periphery formed the friction path, were initially prepared by grinding and lapping. Final preparation consisted of wearing the specimens and friction disc, in the presence of the lubricant used during testing, until their surfaces were as conformal as was thought possible under those conditions. The applied lubricant was exchanged periodically throughout the duration of this final preparation, in order to remove wear debris and ensure the presence of fresh oil at the beginning of a test. The wear-in process was considered complete when its external evidence, the observed values of the coefficient of static friction, which increased during the wear-in process, appeared to reach an upper limit, and when this upper limit existed over the entire periphery of the disc.

Incorporation of a wear-in process was a distinct departure from the procedure of nearly all former investigators of stick-slip oscillation, who have used freshly-prepared (ground or lapped) surfaces for their tests. Wearing-

in of the surfaces, though tedious, offered certain definite advantages. Friction conditions were known to be very uniform over the entire friction track, and to remain stable throughout the duration of a test. Uniformity of conditions, as evidenced by observed friction values, is very unusual in the case of freshly-prepared surfaces, and repeatability of results is impossible to achieve unless the surfaces are refinished after each traversal. Additionally, industrial friction surfaces are most commonly well run-in; numerical results from run-in surfaces have, therefore, greater applicability.

Details of specimen surface parameters may be found in Appendix V.

4.5 Testing Procedure

Correct scaling of instrumentation signals (Appendix IV) was performed prior to the wearing-in of friction surfaces. Immediately upon completion of the wear-in process data concerning variation of frictional properties with tangential load rate was recorded, with load rate application altered in a systematic manner. After the desired speed range had been scanned in this fashion, additional data recordings were made at the initial load rates, in order to ensure that frictional conditions had not suffered any detectable change. At the completion of a test scaling of instrumentation signals was

checked to verify stability of the instrumentation over the duration of the running-in and testing.

It is of particular significance to the conformability of the frictional surfaces that the slider was not removed from the friction path, nor was its orientation in any way disturbed, from the beginning of the wear-in process to the completion of a test.

The major portion of the data was collected by photographing oscilloscope traces. Normal load at the interface was, in all cases, 21.1 pounds.

4.6 Lubricant

Repeated traversals of the friction track made use of a lubricant mandatory if severe scoring of the surfaces was to be avoided. Chemical action between this lubricant and the metallic surfaces was to be avoided, since such action could distort results and obscure the physical mechanisms of boundary friction. Additionally, minimal viscous effect during periods of relative motion was desired, since stick-slip oscillation does not occur if dynamic energy dissipation exceeds a critical level. Greater dynamic energy dissipation results in more rapid decay, on the phase plane, of the slider's phasor amplitude. For persistence of oscillation the slider must, after slip, at a lesser displacement re-achieve the velocity of the other surface. Consequently, at any driven surface velocity v some critical amount of

energy dissipation will exist beyond which the phasor's decay rate is too rapid to permit it to again attain the velocity v, resulting in the continued decay of the slider's phasor to zero amplitude, a state corresponding to non-oscillatory motion of the slider over the driven surface.

The friction surface, during all data runs, was flooded with Liquid Petrolatum (light) B.P., a medicinal-grade napthenic hydrocarbon, or "white mineral oil". This oil does not, in pure form, contain any polar groups, and was therefore, at least nominally, inert with respect to the metallic friction surfaces. Measured viscosity was 120 SSU at 80°F; for purposes of comparison, oil rated at SAE 5W has a kinematic viscosity of approximately 200 SSU at 80°F.

To further avoid undesirable chemical effects, lapping of friction surfaces was performed with a paste made of Liquid Petrolatum and alum powder. No liquid, other than the lubricant, was permitted to contact the surfaces subsequent to the commencement of the lapping procedure. Chemical effects arising from oxidation of the lubricant could not be eliminated, but the repeatability of the results at the initiation and termination of each test suggests that lubricant oxidation, over the period of the few days required for the performance of a test, was not a significant factor.

CHAPTER V

V. DISCUSSION OF RESULTS

5.1 Static Friction

Two photomicrographs, offering clear evidence of simultaneous solid contact and relative motion between opposing friction surfaces, are presented in Figure 5.1.1. Confirmatory surface roughness measurements may be found in Appendix V. That such solid contact exists in the absence of relative motion between surfaces logically follows, since hydrodynamic effects can only increase with relative velocity. The assumption of a solid-contact model for the stick portion of a stick-slip cycle is therefore vindicated, provided, as indicated by the results of Courtney-Pratt and Eisner [9], the portion of the load supported by squeeze film effects is of a lesser order of magnitude than the portion supported by solid contact.

Experimental data showing the variation of the coefficient of static friction with the load rate variable $\dot{\phi}$ is presented, for the steel-on-steel friction couple, in Figure 5.1.2, together with curves defined by the derived equation 3.1.24. Included in Figure 5.1.2, for comparison purposes, is data obtained by Potter [10] for a nominally unlubricated steel-on-steel friction couple using a linear, rather than rotary, apparatus.

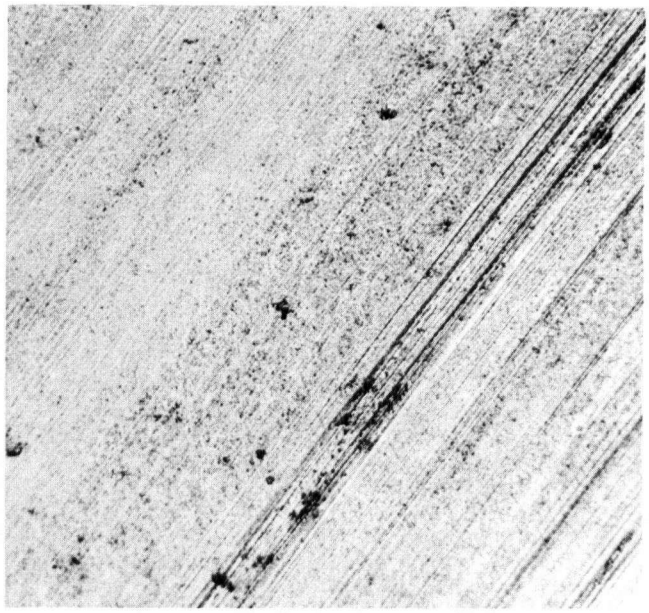

(a) SLIDER SURFACE

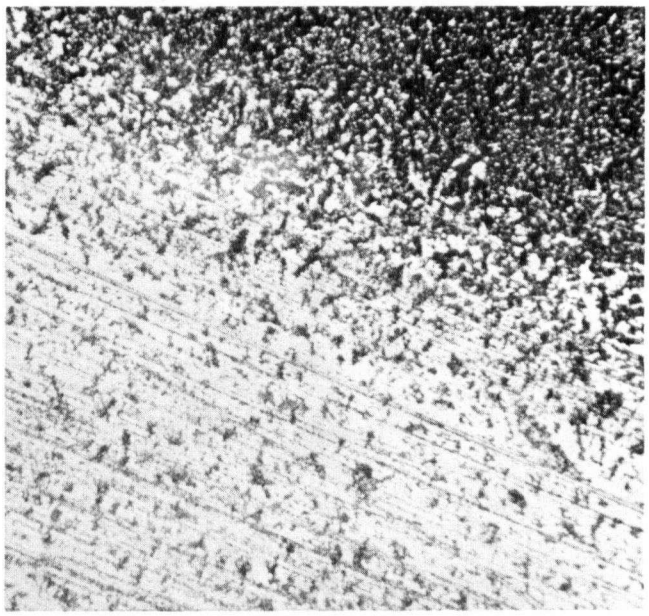

(b) DISC SURFACE

Figure 5.1.1 Post-Test Photomicrographs of Slider Surface and Friction Disc Surface (Steel-on-Steel), X75

Directional wear markings are plain on both surfaces. Pre-test lapped surface finish is evident in right-hand upper corner of Friction Disc Surface photomicrograph

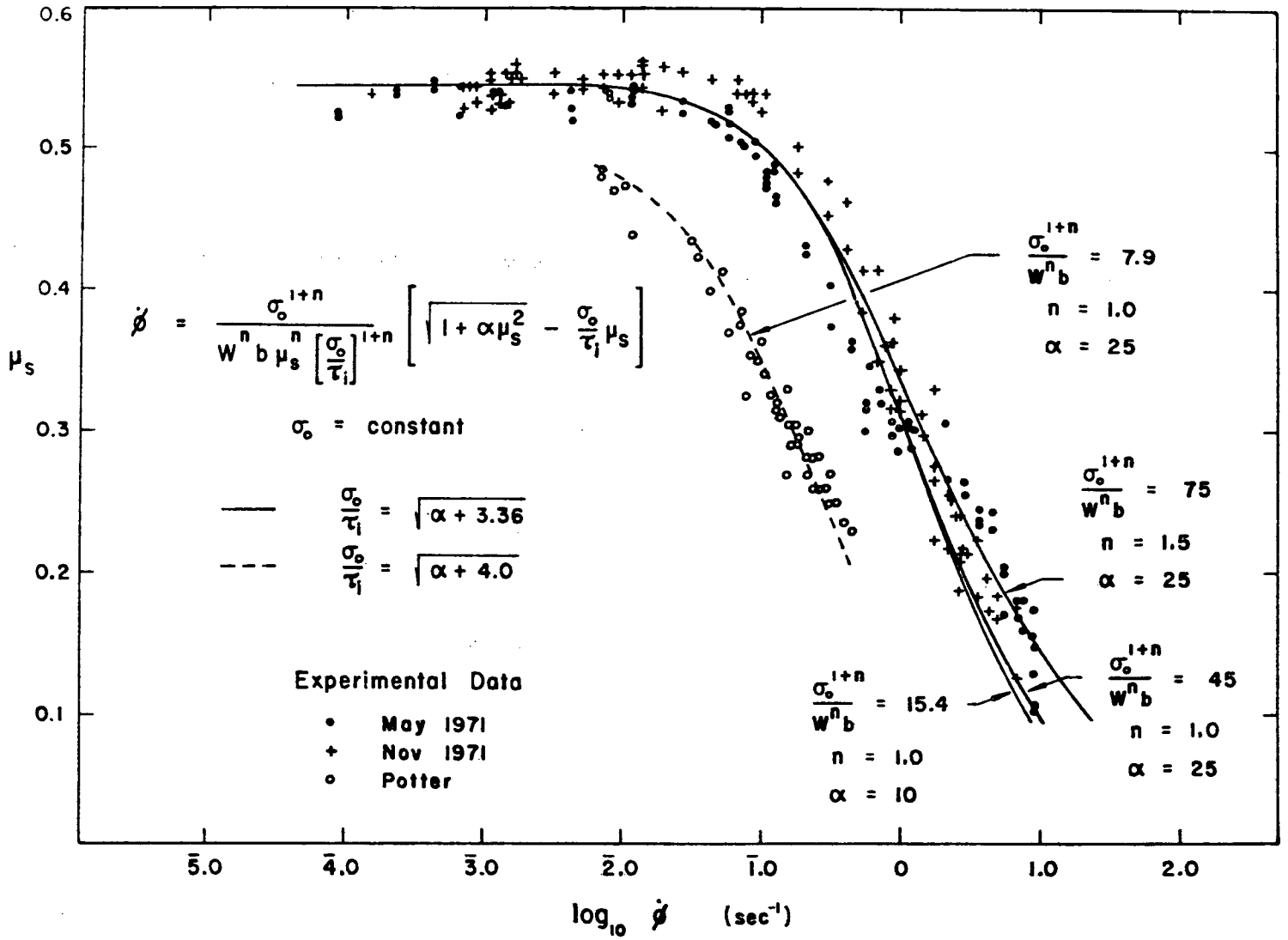

Figure 5.1.2 Variation of the Coefficient of Static Friction with Load Rate Variable $\dot{\phi}$, Steel-on-Steel

In the derivation of equation 3.1.24 the term $\frac{A_s}{W} \dot{\tau}_i$ was assumed negligibly small compared to the load rate variable $\dot{\phi}$: this assumption must now be verified.

The postulated mechanism of asperity deformation and area growth, plastic deformation resulting from application of a ramp form of tangential load (in combination with a constant normal load), permits the assumption that the rate of strain in an asperity is approximately proportional to the load rate variable $\dot{\phi}$. A further assumption that strain at slip (fracture) is approximately 1 in/in, both in the present investigation and in the tensile experiments of Nadai and Majoine [27], in combination with time of stick data from the present investigation, yields the result that $\dot{\phi}$ and the tensile strain rate $\dot{\varepsilon}$, as presented in Figure 3.1.4, are of the same order of magnitude. In other words, data from Nadai and Majoine, for a given magnitude of $\dot{\varepsilon}$, should be applicable to an approximately equivalent magnitude of $\dot{\phi}$.

The ratio $\frac{A_s}{W}$ is identical to $\frac{\mu_s}{\tau_i}$. Both quantities in this second ratio are readily obtained from data. The time derivative $\dot{\tau}_i$ may be approximately calculated, again assuming fracture strain to be 1 in/in, by computing $\dot{\tau}_0$. In the load rate range $\dot{\varepsilon} = 10^{-4}$ to 10^{1} sec^{-1} $\frac{A_s}{W} \dot{\tau}_i$ can be shown, for mild steel, to be at least two orders of magnitude less than the corresponding strain rate $\dot{\varepsilon}$. Hence, over the same range of $\dot{\phi}$, the term $\frac{A_s}{W} \dot{\tau}_i$ is also two orders of magnitude less than its corresponding load rate $\dot{\phi}$. The initial assumption,

$\frac{A_s}{W}\dot{\tau}_i$ is negligibly small in comparison to $\dot{\phi}$, is consequently justified for low-strength steel.

In the fitting of equation 3.1.24 to the experimental data, the static friction coefficient at zero load rate $\mu_s\Big|_{\dot{\phi}=0}$ was assumed to be the value of the apparent upper asymptote, $\mu_s = 0.55$. Substitution in equation 3.1.22 yields

$$\frac{\sigma_0}{\tau_i} = \alpha + 3.36 = 5.3, \quad \alpha = 25 \qquad = 3.7, \quad \alpha = 10 \tag{5.1.1}$$

The experimentally-deduced value of σ_0/τ_i is obviously strongly influenced by the assumed value of α. Interestingly, because the constant K in equation 3.1.16 should not be substantially less than unity, comparison of equations 3.1.6 and 5.1.1 favours choosing α to be approximately 25, reinforcing the conclusions of Greenwood [45].

For purposes of this study, the value of α, though valuable if it could be precisely determined, is not of paramount importance. Examination of Figure 5.1.2 will reveal that a change of α, within a feasible range, has only a minor effect on the profile of the static friction response curve. A change in α does, however, shift the response curve to right or left on the logarithmic load rate axis, necessitating a compensating change in the location parameter $\sigma_0^{1+n}/W^n b$; determination of this parameter is, therefore, contingent upon knowing the value of α.

The upper limit of the power index, n = 1.5, would correspond to uniform deformation throughout the volume of material within the elastic-plastic boundary. The lower limit, n = 1.0, would correspond to uniform deformation along some front advancing with the boundary of the contact; such a front might occur at the elastic-plastic boundary if the plastic material was restrained in the direction normal to the free surface. Examination of Figure 5.1.3 will reveal that n might be expected to have an effective value equal to neither of these two limits, but rather, some intermediate value. Although determination of n could be of significance to further understanding of the area growth phenomena, the insensitivity of the response curve profile to changes in n, as well as in α, together with the scatter of the experimental data, prevents any statement more conclusive than that the previously-stated limits appear consistent with the available information.

Variation in n, unfortunately, also causes lateral shifts in the static friction response curve. Determination of the value of the location parameter $\sigma_0^{1+n}/W^n b$ is consequently doubly difficult, since it relies on accurate knowledge of both n and α.

Before terminating discussion of the information presented in Figure 5.1.2, it is significant to the general applicability of the present theory that the static friction response curve profile of equation 3.1.24 fits the data of

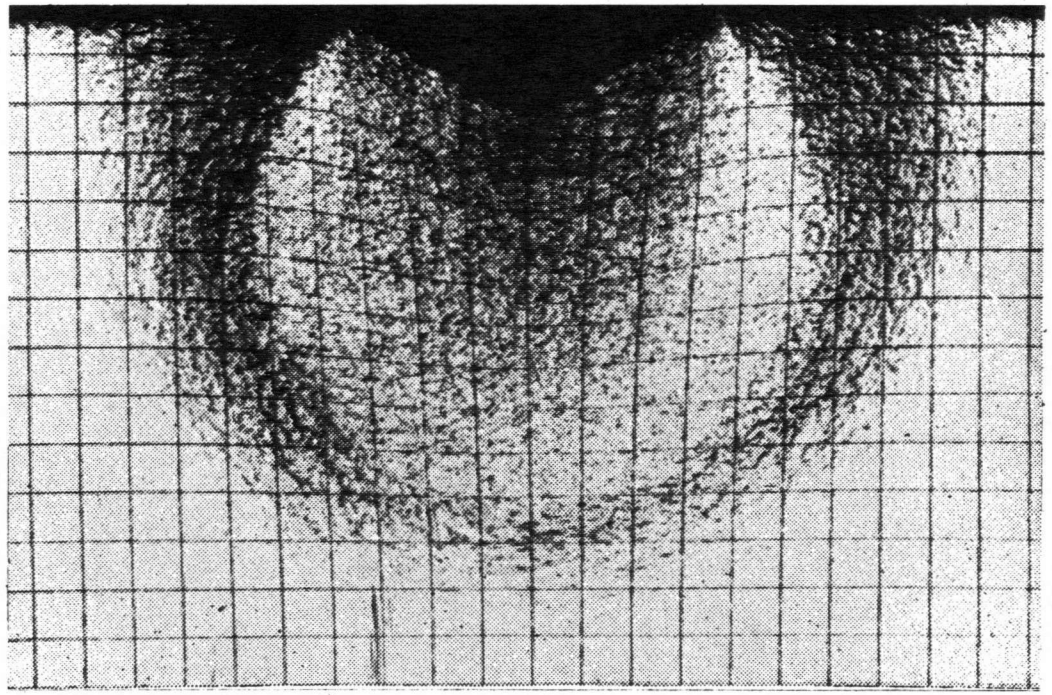

Figure 5.1.3 **Zone of Deformation beneath a Longitudinal Wedge Indentation [44]**

Note hemispherical contour of elastic-plastic boundary and non-uniform nature of deformation within boundary

Potter, which exhibits both a wide range of static friction values and the first indications of an upper asymptote, as capably as it does data collected during this study, if the limiting static friction value $\mu_s\Big|_{\dot{\phi} = 0}$ is reduced to 0.50. The ability of equation 3.1.24 to describe these data sets reinforces the initial supposition that, during stick, solid contact is the dominant load-bearing mechanism, and the consequent omission of squeeze-film effects from the analytical model. The quantity of liquid lubricant displaced by the decrease in mean surface separation during stick must consequently have experienced very little difficulty in exiting the interfacial zone, at the rates required, through the flow passages between asperity contacts.

During the testing of brass on steel, metallic transfer from the brass slider to the steel disc occurred, as evidenced by the photomicrograph presented in Figure 5.1.4. No evidence of material transfer from the steel disc to the brass slider was detectable. One might consequently expect frictional behaviour to be dominated by the more physically active of the two metals, brass.

That brass was, in fact, the more physically active of the two surfaces is worthy of note. If, for whatever reason, a contact junction should possess an ultimate shear strength in excess of that of either metal matrix, fracture will occur, not at the interfacial junction, but in the weaker matrix. Transfer might have been expected from the steel,

DISC SURFACE

Figure 5.1.4 Post-Test Photomicrograph of Friction Disc Surface (Brass-on-Steel), X250

Metallic transfer of brass to the steel friction disc surface is evident

the weaker of the two materials at room temperature (steel 55 kpsi UTS, brass 75 kpsi UTS, approximately), to the brass. That transfer occurred in an inverse manner suggests that, at the time of shear, the strength of the brass at the points of transfer was less than that of the steel. Perhaps thermal effects, such as were reported by Bowden and Ridler [4], would provide an explanation for this apparent reversal of relative strengths. The brass material, as received and employed, was highly cold-worked; heat generated at the interfacial surfaces, whether during stick or slip, might well have partially annealed the relevant surface portions of the brass specimen, resulting in local regions wherein the shear strength of the brass was less than that of the steel or the interfacial junction. Conversely, cold-working of the surface of the annealed steel might have sufficiently increased its shear strength, in these surface regions, so that the effective shear strength of the steel exceeded that of the cold-worked brass. Whatever the explanation, the properties of the brass surface may be expected to govern the observed frictional behaviour.

Specific data on the fracture strength of brass, under conditions of varied stress rate, or even varied strain rate, has not been located. The most valid comparative data available is that presented, for copper, in Figure 3.1.3. As has been stated, the response of the ultimate strength of brass to varying strain rate might, in the absence of better

information, be assumed described by equation 3.1.25, but the rate of shearing strain in an asperity junction is unknown, precluding direct use of this equation.

The metal at the asperity junction is, for the postulated mechanism, marginally plastic. For this condition of plasticity the rate of shearing strain, at the interface, may be considered proportional to the rate of horizontal load application, at least as a first approximation, so that

$$\sigma_0 \cong K \dot{\phi}^m \quad . \tag{5.1.2}$$

Substitution of equation 5.1.2 into equation 3.1.23 results in the graphical plots exhibited in Figure 5.1.5, together with the data obtained for variation of static friction coefficient with load rate. The plot for which m equals zero (σ_0 = constant) is quite inadequate to describe the data, whereas, if m is of the order 0.1 a very respectable matching of derived plot and data is achieved.

Examination of Figure 3.1.3 will reveal that, for copper, the power index m has a value of the order of .02, approximately one-fifth of the value required to match the profile of equation 3.1.24 to that of the data for the brass-on-steel friction pair. This difference in magnitude is not beyond credibility when one considers how drastically the physical properties of a metal can change when it is alloyed.

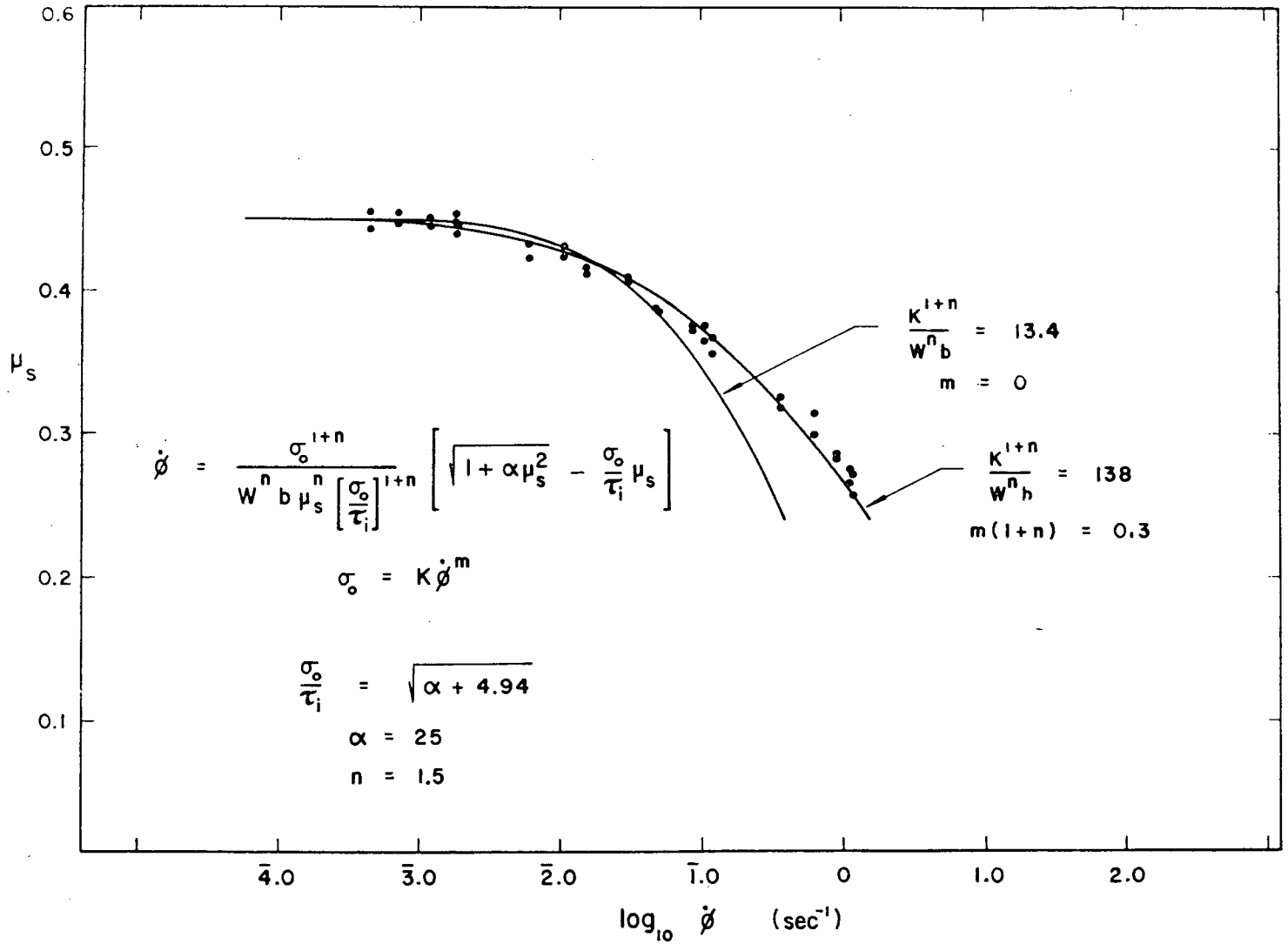

Figure 5.1.5 Variation of the Coefficient of Static Friction with Load Rate Variable $\dot{\phi}$, Brass-on-Steel

Specifically, the difference in magnitude of the power index m could be attributed to the fact that dislocation movement in brass, which has substitutional zinc atoms in a copper lattice, is more restricted than dislocation movement in pure copper.

For the copper data presented in Figure 3.1.4, the term $\frac{A_s}{W}\dot{\tau}_i$ in equation 3.1.20 can be shown to be, throughout the range of load rates spanned by this investigation, three orders of magnitude smaller than the load rate variable $\dot{\phi}$. The assumptions and method of analysis are identical to those employed in determining the relative magnitude of those terms for the case of steel-on-steel frictional contact. The difference in magnitude of the power indices m, for copper and brass, indicates that, for brass, $\dot{\phi}$ would be only two orders of magnitude greater than $\frac{A_s}{W}\dot{\tau}_i$, but that difference is still entirely adequate for assurance that $\frac{A_s}{W}\dot{\tau}_i$ is negligible throughout the experimental load range. This assumption is therefore validated for the brass-on-steel, as well as the steel-on-steel, friction pair.

In summary, two ductile metals, brass and steel, have been tested under boundary friction conditions on a steel surface. Both material combinations showed definite upper limits of static friction in the presence of a lubricant, and the behaviour of both friction pairs, when subjected to varied rates of tangential stress application, appears adequately described by the developed equation 3.1.24.

5.2 Kinetic Boundary Friction

a. Slip

The established form of the friction force curve during slip, as determined by Bell and Burdekin [12], is represented schematically in Figure 2.1.2. The maximum value of friction force, which determines the coefficient of static friction, corresponds to conditions at the incidence of slip. Once slip was initiated, the friction force magnitude fell while relative surface velocity increased to a maximum; as the relative velocity decreased from maximum to zero, the friction force remained univalued.

The form of friction force trace reported by Bell and Burdekin has been recorded during the course of this study, and a representative data recording of this type, for the steel-on-steel friction pair, may be found in Figure 5.2.1. The lower surface velocity during generation of this recording was 2.8×10^{-2} in/sec; the achieved coefficient of static friction was 0.26. This form of trace is not, however, invariant. As the lower surface velocity was reduced, in order to achieve greater coefficients of static friction, the phase plane displacement and friction traces altered progressively to the forms displayed in Figure 5.2.2. Unlike the traces displayed in Figure 5.2.1, these recordings were made sequentially; static friction values achieved differed slightly, but there is no doubt concerning the repeatability and mutual compatibility of the friction force and displacement traces.

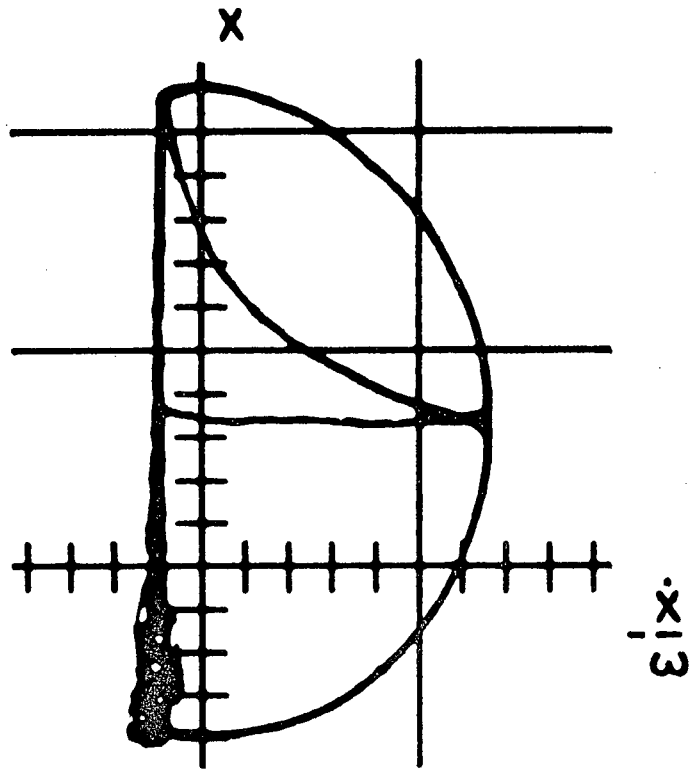

Figure 5.2.1 Recorded Half-Cycle Stick-Slip Phase Plane Traces

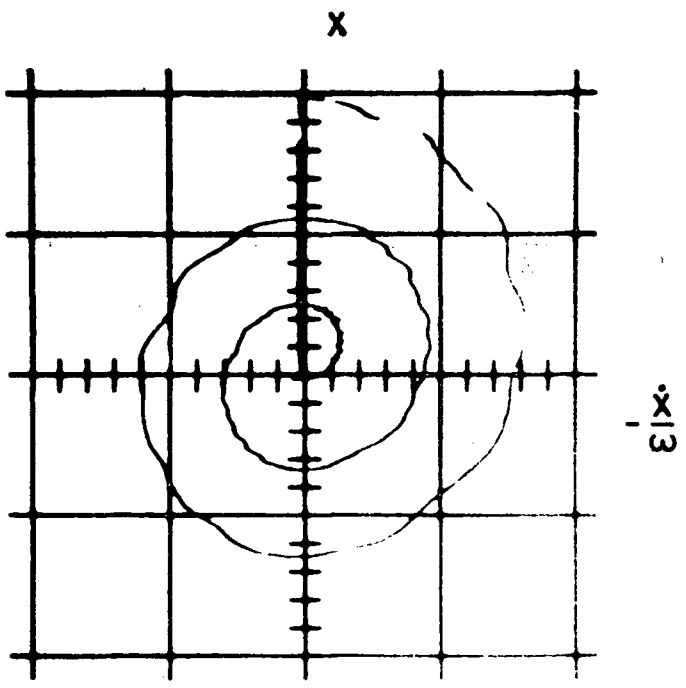

$v = 0.11$ in/sec

$\mu_s = 0.48$

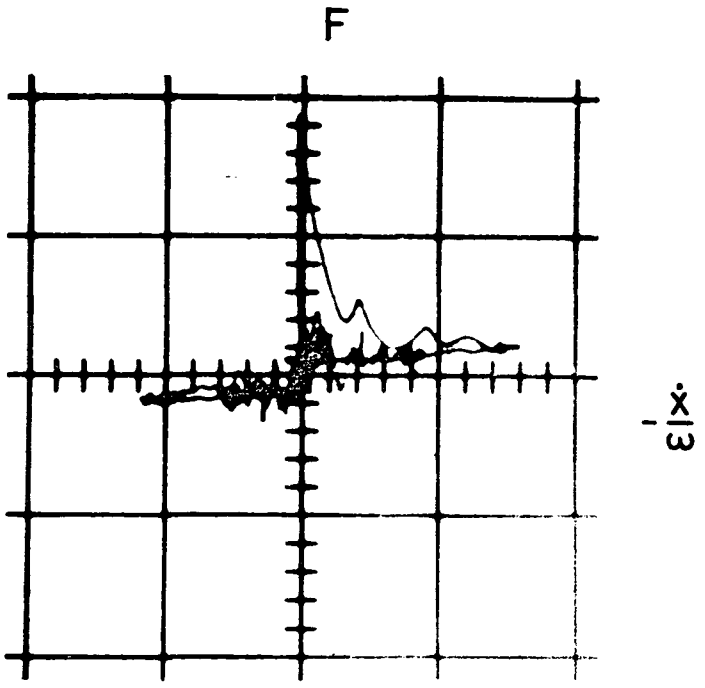

$v = 0.11$ in/sec

$\mu_s = 0.45$

Figure 5.2.2 Recorded Multi-Cycle Stick-Slip Phase Plane Traces (Steel-on-Steel, 100 mv/div)

Several significant observations result from examination of the traces of Figure 5.2.2. Traditional stick-slip theory postulates that the slip portion of the displacement trace should be a half-cycle because the surfaces would re-attach as soon as their relative velocity fell to zero. This re-attachment was supposed to occur because the restoring force at the time when the surface velocities matched, after an energy-dissipating half-cycle, should be less than that required to overcome static friction. This explanation, which ignores rate effects, is somewhat oversimplified; it is sometimes applicable, but Figure 5.2.2 plainly shows that its application is far from universal, since the restoring force at the end of two cycles, which corresponds to a frictional coefficient of 0.12, still exceeds in magnitude the forces favoring re-attachment.

Perhaps the most significant revelation of Figure 5.2.2 is that the upper portion of Bell and Burdekin's dual-valued friction curve is a transient which exists only before the system achieves stable slip conditions, as defined by the lower portion of the friction curve. This stable lower portion of the friction curve traditionally exhibits a Coulombic form, but that of Figure 5.2.2 shows both Coulombic and viscous characteristics, suggesting that both mechanisms of friction are active. Specifically, the curve suggests the presence of both solid-contact and viscous modes of energy dissipation. That the surfaces should have solid contact

has been demonstrated by the conductivity studies of Green [16]; that viscous effects should be added to the solid-contact effects in the presence of a liquid lubricant is not unexpected.

The value of the observed friction force at zero relative velocity, where viscous drag is zero, corresponds to a friction coefficient of approximately 0.03. Steel-on-steel contacts, using mild steel, have been found to have a minimum kinetic friction coefficient, at low speeds and in the presence of highly effective boundary lubricants, of 0.053 [34]. Because the lubricant used in this study was chosen for its poor boundary lubrication properties, some physical mechanism other than solid contact was obviously responsible for the reduction of the kinetic friction to the level observed, a reduction which could occur only if some portion of the normal load was not supported by solid contact. That part of the normal load was supported by the viscous liquid film, even at zero relative velocity, appears inescapable.

The existence of a load-bearing squeeze film at the primary matching, after slip initiation, of surface velocities suggests that this film must have been established during the first half-cycle of slip. That lubricant is present between the surfaces during the terminal stages of stick, interspersed in the free volume between asperity contacts, is certain, but because the interfacial gap is greater (area of contact smaller) during slip than during stick, this

residual volume of lubricant is insufficient to form the viscous squeeze film observed during slip. An additional volume of lubricant, greater than that to be expected if the normal load was entirely supported by solid contact, collected between the friction surfaces during the first half-cycle of slip. The source of this additional lubricant is no mystery, since the friction surface over which the slider moved was flooded with oil. The source of the lifting forces experienced by the flat slider is less obvious. Hydrodynamic lift, which nominally requires the existence of a convergent surface gap, would initially appear to be inoperative, in this investigation, as a result of the carefully-maintained parallelism of the slider and disc faces. Recall, though, that hydrodynamic lift does exist in just such cases, and is certainly the most plausible source of lifting forces under the experimental conditions of this study.

If present during the first half-cycle of slip, hydrodynamic lift must also have been present during the remainder of slip. The stability of Figure 5.2.2, for a duration of two cycles, would suggest that the lift is due to surface rugosity, and not to a transitory thermal expansion of the lubricant or short-term thermal deformation of the surfaces. Although insufficient to form a squeeze film, the residual lubricant between the surfaces during stick would be sufficient to generate hydrodynamic lift between closely approaching asperities, since such lift generation

requires only lubricant in the microscopic regions of convergency. Such lift would effect the entrance of more lubricant beneath the slider, allowing the continuation of the process to a state of equilibrium. Note also that the magnitude of friction values over the stable portion of the friction force trace was reduced if the slider travelled a greater distance over the lower surface before stable conditions were achieved, a fact compatible with the concept that hydrodynamic lift causes the establishment of an increasingly thicker fluid film during the transient portion of slip.

In order to further investigate transitory characteristics of slip, transition curves recorded at a variety of lower surface velocities were graphically compared. The curves were normalized with respect to the value of friction at which they met the stable kinetic friction curve, in order that only transitory behaviour might be studied, and plotted as functions of time, relative velocity, and displacement of the slider with respect to the lower surface. These plots, which may be found in Figures 5.2.3 to 5.2.5, suggested strongly that distance travelled by the slider was the dominant variable governing the rate of decay of the transitory kinetic friction. Further confirmation of this finding was provided by increasing the system's natural frequency of vibration to 152 rad/sec by removing the lead weights from the end of the beam. Undesirable dynamic imbalance and reduction of vibrating mass

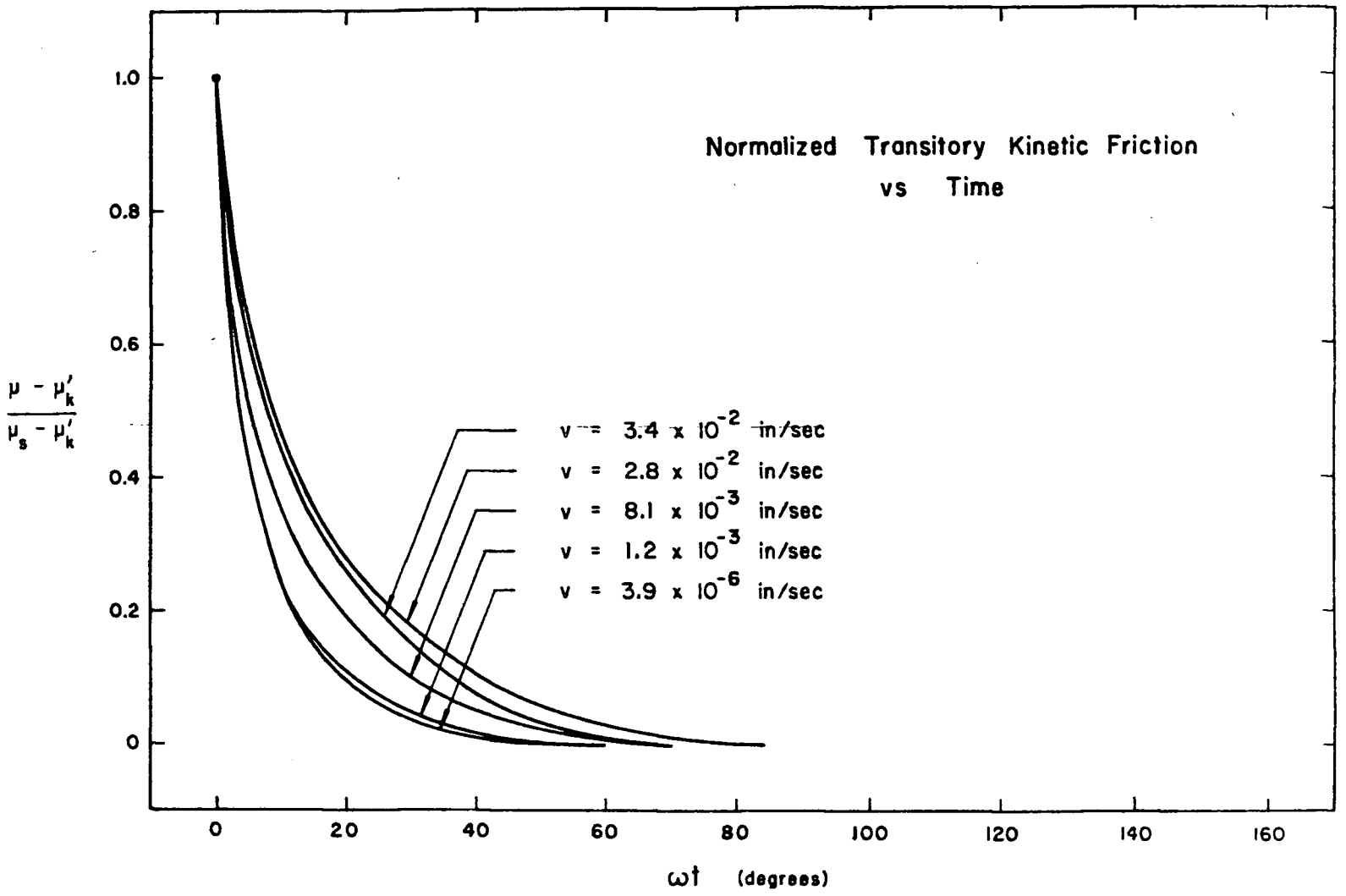

Figure 5.2.3 Normalized Transitory Kinetic Friction vs Time (Steel-on-Steel, ω_d = 102 rad/sec)

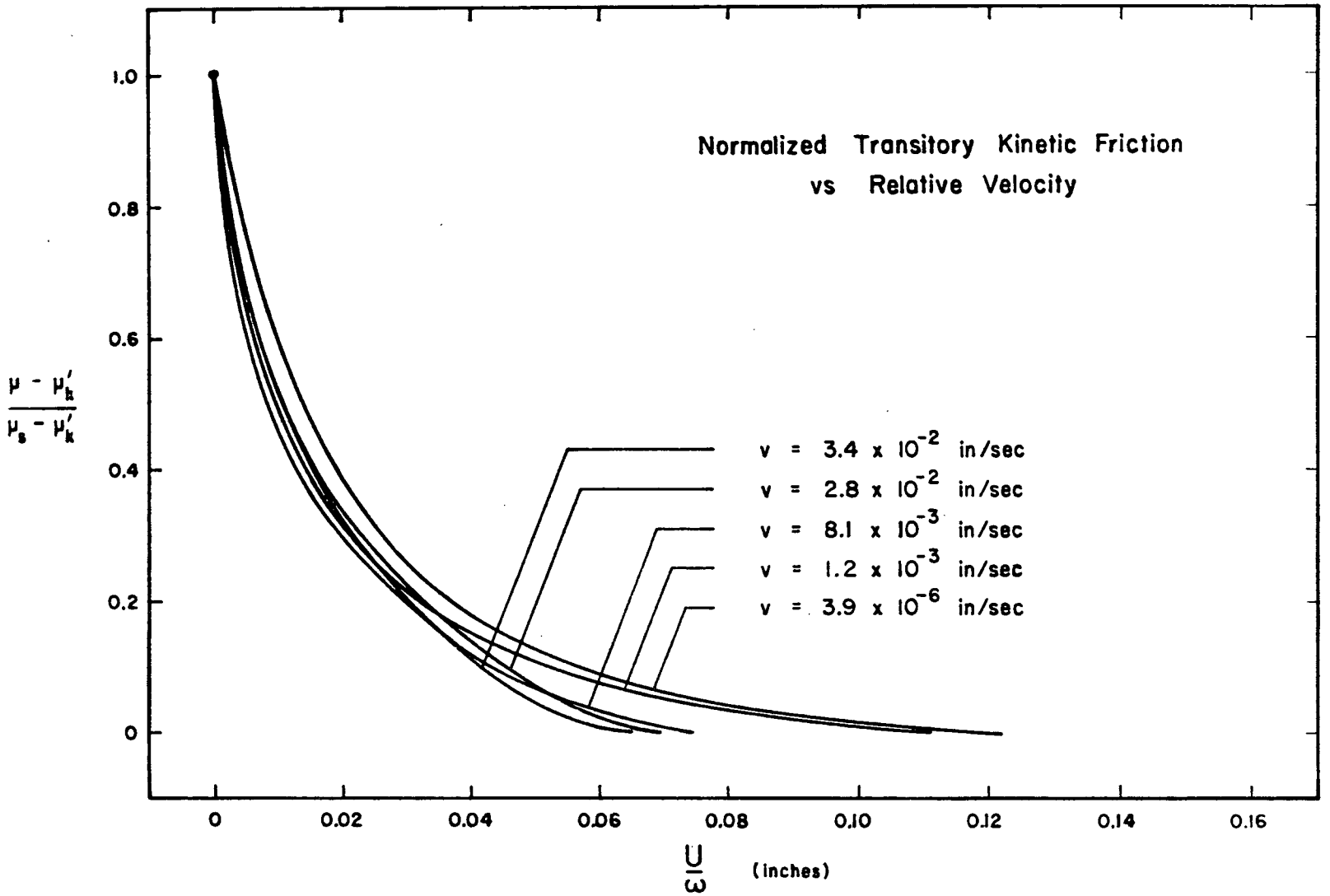

Figure 5.2.4 Normalized Transitory Kinetic Friction vs Relative Velocity (Steel-on-Steel, ω_d = 102 rad/sec)

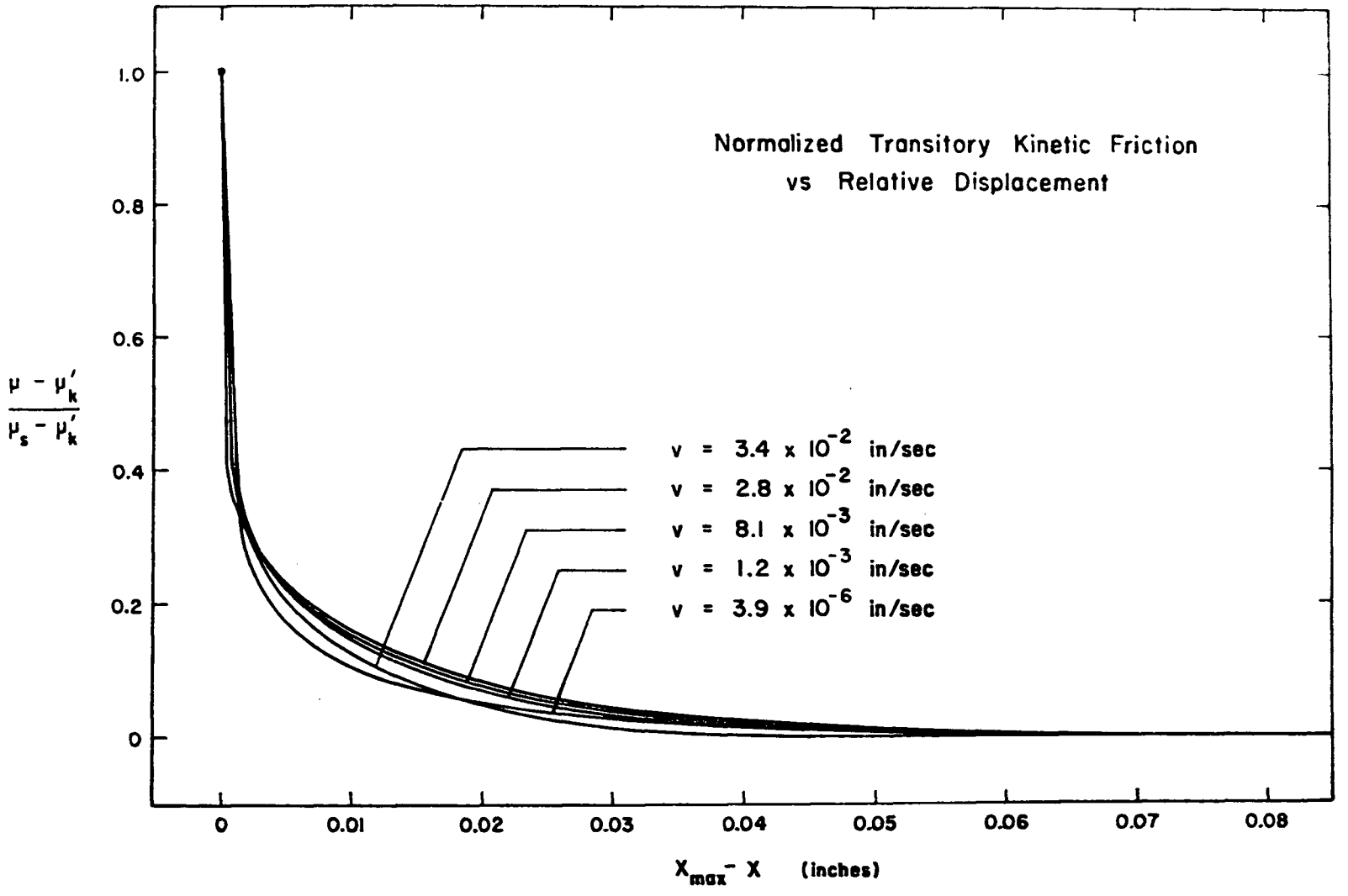

Figure 5.2.5 Normalized Transitory Kinetic Friction vs Relative Displacement (Steel-on-Steel, ω_d = 102 rad/sec)

concentration resulted in imperfect phase lags between the instrumentation signals, as well as introducing the possibility of non-parallel dynamic orientation of the friction surfaces, but the information gained provided valuable support for the findings of the graphical transitory plots. Comparison of the friction force curve (Fig. 5.2.6) with that presented in Figure 5.2.1 again indicates, despite small out-of-phase effects evident in the recording of a slightly positive velocity during the first quarter-cycle of slip, that there is little basis for considering the rate of decay of the transition to be directly governed by either velocity or time. The recorded curves of friction force versus displacement, however, show startling similarity for the two natural frequencies. This similarity, together with the similarity of the normalized friction curves of Figure 5.2.5, forces the assertion that the decay rate of the transitory portion of the kinetic friction curve is apparently governed by the distance travelled by the slider over the lower surface.

The distance travelled at the termination of the transient portion of the slip cycle is many orders of magnitude greater than the size of any practical asperity. The transition cannot, therefore, correspond to progressive fracture of the asperity contacts formed during stick, as former investigators have suggested. Remember, however, that the slider and its supporting structure possess inertia in the normal, as well as tangential, plane and that the strain during stick is such

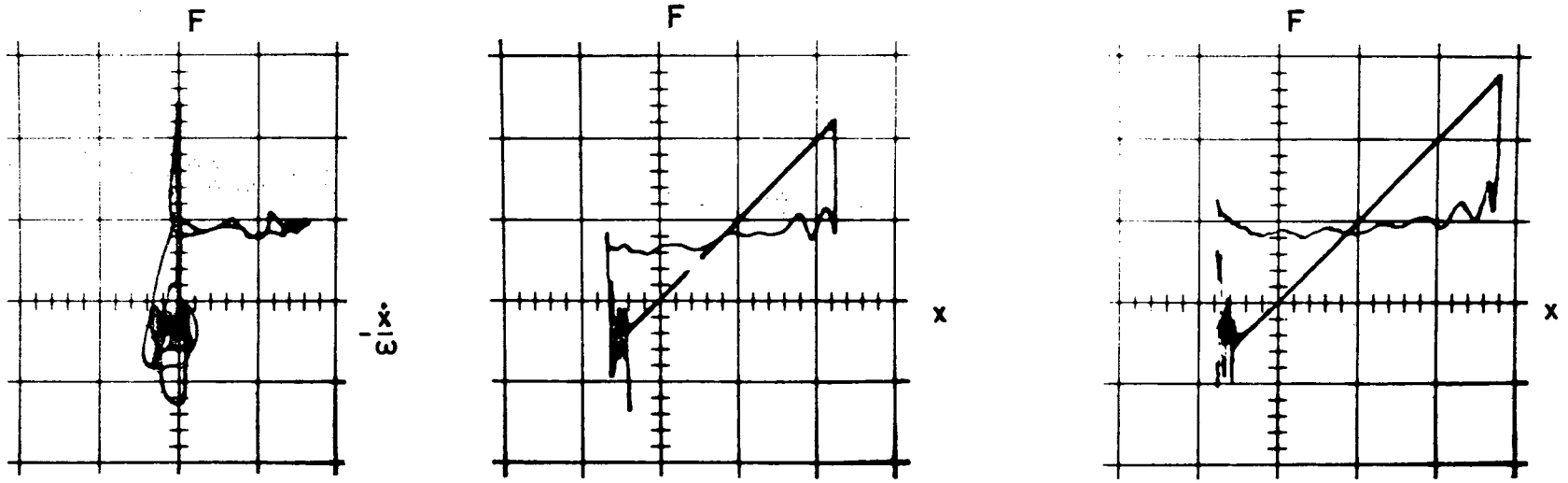

Figure 5.2.6 Recorded Transient Slip Traces (Steel-on-Steel)

that the center of mass of the slider is displaced toward the lower surface. This inertia, with respect to perpendicular movement, ensures that although the asperity junctions formed during stick might all have fractured, the area of contact at the inception of slip cannot be instantaneously reduced, despite the encouragement of such area reduction by the decreased total surface stress and the growing fluid film. Unfortunately, the transitional decay rate cannot be correlated with time, as it would be if inertia normal to the surface dominated the behaviour; removing the lead weights from the end of the beam altered the system's moment of inertia for that plane by less than 3%. The interaction of forces during this important portion of the slip cycle is obviously complex, and would be worthy of much closer attention than the scope of this study permits.

In summary, the slip portion of the stick-slip cycle begins when, during stick, the applied tangential shear stress exceeds the fracture strength of the real contact area. Slip progresses through a complex transitory regime, correlatable with relative displacement of the surfaces, during which the area of contact is drastically reduced and, in the presence of a liquid lubricant, a load-bearing fluid film is established by hydrodynamic action on a microscopic scale. The transitory slip condition decays to a stable state of slip wherein the normal load is supported partially by solid contact, partially by the fluid film. Because effective surface separation is

of the order of the height of a surface asperity, squeeze film effects assure the persistence of this fluid film for the short periods (milliseconds) when hydrodynamic lift is negligible due to inadequate relative velocity. The slip portion of a vibratory cycle terminates at the first matching of surface velocities after frictional energy dissipation has reduced the corresponding displacement, whether positive or negative, sufficiently that the sum of the forces favouring reattachment of the surfaces exceeds the elastic restoration force. Upon reattachment of the surfaces another period of stick commences. If the velocity of the driven surface is sufficiently great that the forces favouring reattachment do not exceed the elastic restoration force before the maximum positive velocity of the oscillating surface becomes less than the driven surface velocity, reattachment cannot occur, and stick-slip oscillation disappears. Non-oscillatory sliding of the elastically-mounted surface, at a fixed displacement proportional to the magnitude of the kinetic traction forces, ensues.

b. Quasi-Harmonic Oscillation

Slip and quasi-harmonic motion are distinctive entities because, although the friction forces encountered during slip are entirely dissipative, dynamic friction forces causing quasi-harmonic oscillation are not. The "humped" form of friction force vs velocity curve reported by Ko [15] to be characteristic of quasi-harmonic oscillation, one form being

that shown in Figure 2.1.3, may be energy-additive, energy-dissipative, or both (Appendix II), depending on the velocity of the driven surface.

An example of a humped friction curve, together with a generated behavioural trace, is presented on the phase plane in Figure 5.2.7.

Inherent in the balancing of additive and dissipative energy effects to achieve a stable, quasi-harmonic limit cycle is the necessity for the zero axis of absolute velocity of the driven surface to fall in the immediate vicinity of the "hump" of the curve. If this hump and the zero velocity axis are too widely separated the dissipative and additive energy effects will not balance, negating the achievement of a stable limit cycle. A related point of significance is that the positively and negatively sloped portions of the friction-velocity curve need not have the relative positions illustrated in Figure 3.3.1 for achievement of a stable limit cycle. If, instead, the friction-velocity curve has a minimum, rather than maximum, value in the vicinity of the zero velocity axis, due to reversal of the relative positions of the sloped portions of the curve, a stable limit cycle is still achieved. The sole criterion for the endurance of such a limit cycle is that the cycle must encompass balanced proportions of energy-additive and energy-dissipative zones on the friction-velocity curve.

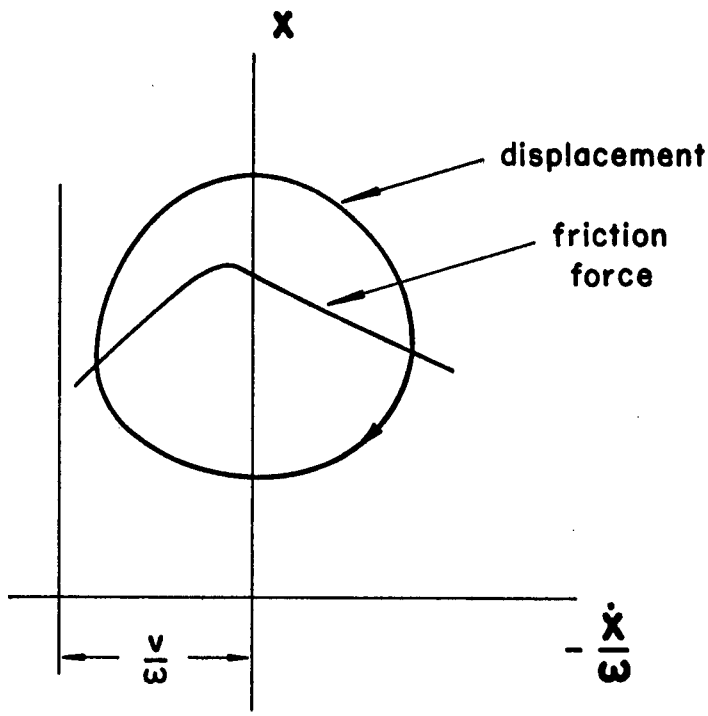

Figure 5.2.7 One Form of Quasi-Harmonic Friction Force Phase Plane Trace, with Generated Displacement Behavioural Curve

Ko has proven that the form of the friction force vs velocity curve recorded during quasi-harmonic oscillation may be either convex upward or convex downward. This basic change in friction curve profile was accomplished simply by changing lubricants. Other researchers have found that similar drastic changes can be made in the non-vibratory boundary friction force vs velocity curve simply by changing the additives in an otherwise homogeneous base oil [35,36]. It is of importance that highly-refined mineral oil has been found to exhibit only a convex upward primary inflection, similar to the example of Figure 5.2.7, both in the work of Ko and in the present study. The inverted, convex downward form of the friction force vs velocity curve would therefore appear to result from the presence of oil additives.

A representative set of quasi-harmonic displacement and friction force phase plane traces, recorded during the present study, may be found in Figure 5.2.8. Included are zero reference lines for displacement and force, since locating zero for both curves at the origin of the oscilloscope grid, as was done for all stick-slip recordings, would have resulted in a partial overlay of the traces.

The striking resemblance of the quasi-harmonic friction force curve to Crook's plots of elastohydrodynamic kinetic friction coefficient versus velocity (Fig. 3.2.3) is immediately apparent. This resemblance is hardly startling; the lubricants were similar, and local pressures at the load-bearing extrem-

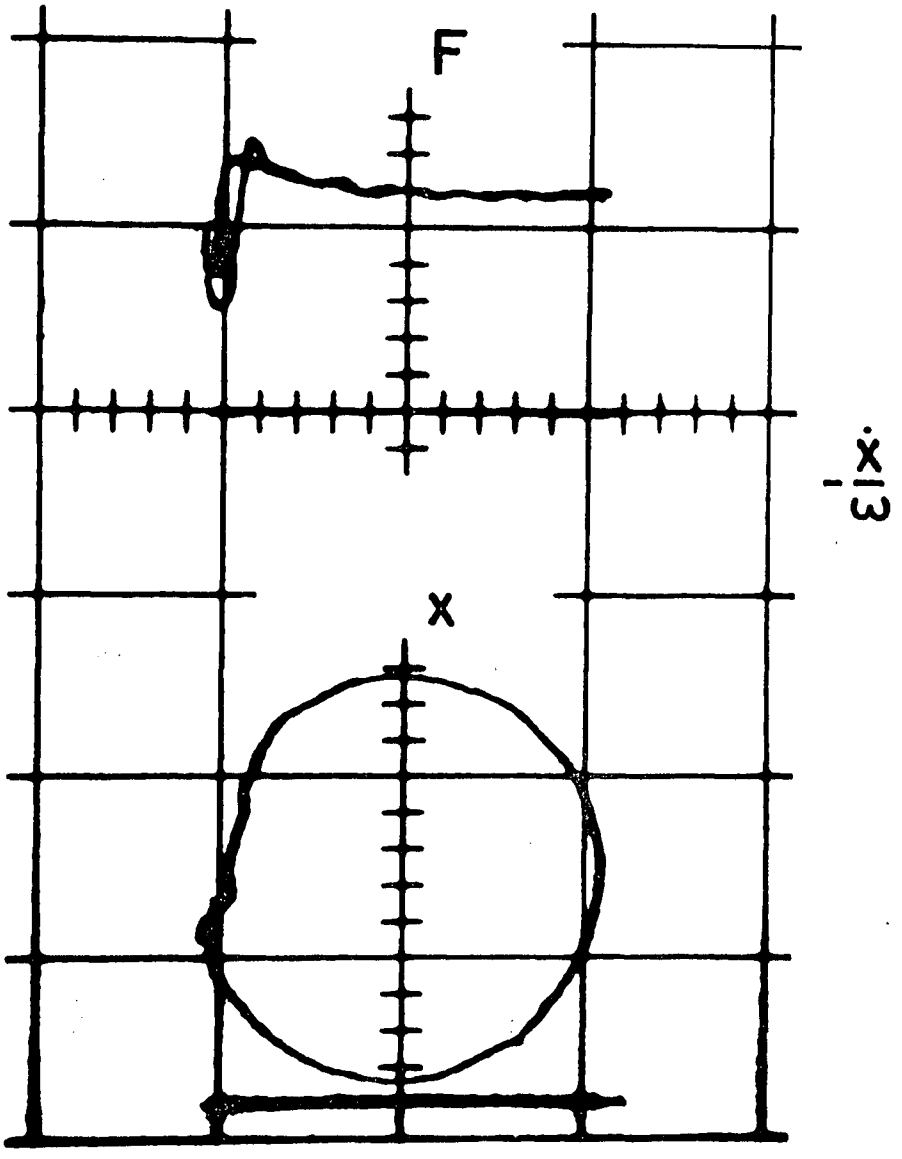

Figure 5.2.8 Recorded Quasi-Harmonic Phase Plane Traces (Steel-on-Steel, 50 mv/div, ω_d = 102 rad/sec, v = 5.3 in/sec)

ities of the quasi-harmonic boundary friction surfaces were of the same order as the film pressures of Crook's experiments. Important differences do, however, exist in the results. The near-horizontal portion of the quasi-harmonic friction force curve corresponds to a kinetic friction coefficient of approximately 0.15, with the force curve maximum occurring at a relative surface velocity of 1 in/sec. The near-horizontal portions of the elastohydrodynamic kinetic friction curves have an approximate coefficient magnitude of 0.03, with maxima occurring at 20 in/sec.

The most significant of the differences between the friction curves of the two studies is their coefficient magnitude ratio of 5. The elastohydrodynamic friction curves of Crook have magnitudes which suggest little, if any, solid contact between opposing surfaces. Hydrodynamic lubrication is also apparent in the way that the friction forces approach zero with relative velocity. These hydrodynamic conditions resulted from the maintenance of high surface velocity, during all tests, on at least one surface, in conjunction with the obvious liquid wedge effect of parallel cylinders with surface velocities, in the load-bearing region, of the same sense. The magnitude of the quasi-harmonic friction coefficients, however, together with the distinctly positive friction force as relative velocity approaches zero [14], indicates that the majority of the load is supported by solid contact during this form of vibration, and that the effective minimum clearance

h_{min} for quasi-harmonic oscillation is much less than its elastohydrodynamic counterpart. The variation in the quasi-harmonic kinetic coefficient of friction would appear to be the result of a minor portion of elastohydrodynamic action superimposed on the dominant solid contact effects.

At any given velocity, an increase in the coefficient of friction results in greater heat generation. How much the lubricant viscosity is affected by the increased rate of heat generation depends greatly on the ability of the friction surfaces to conduct the heat away from the lubricant, but one can confidently state that, since the maximum of an elasto-hydrodynamic friction curve is fixed by viscous temperature effects, this maximum will occur at a lower surface velocity for increased friction coefficient magnitudes. Friction forces resulting from simultaneous viscous and metallic sources are much higher, with proportionately greater heat generation, than those caused by viscous sources alone. The occurrence of the friction force peak at a surface velocity, in quasi-harmonic oscillation, one-twentieth that at which it occurred in Crook's investigation is thus consistent with the concept that the quasi-harmonic friction curve is the result of superimposed elastohydrodynamic and metallic contact effects.

To summarize, it is possible that the form of friction force vs velocity relationship found to cause quasi-harmonic oscillation when using highly refined mineral oils as lubricants results from the superposition of solid contact and

elastohydrodynamic friction force vs velocity characteristic curves to yield the required "humped" form of frictional behaviour, with the maximum designated as the "hump" attributable, in the absence of chemical lubricant additives, to variation in lubricant viscosity as a consequence of thermal sensitivity.

c. Quasi-Steady Viscous Thermal Effects

The similarities in the observed frictional characteristics of elastohydrodynamic lubrication and the viscous contribution to quasi-harmonic behaviour have been outlined, and the observed differences resolved by consideration of the effect that superimposed metallic solid contact would have on the elastohydrodynamic friction curve. One apparent anomaly is yet unexplained. If, indeed, the maximum of the quasi-harmonic friction force curve, which occurs at a relative velocity of 1 in/sec, is caused by thermal variation of lubricant viscosity, as is that of elastohydrodynamic lubrication, why is there no similar maximum in the stable friction curve of slip, during which surface velocities greatly exceed 1 in/sec?

Comparison of the results displayed in Figures 5.2.1, 5.2.2, and 5.2.8 reveals that, as the lower surface velocity v, the average relative speed of the two friction surfaces, is increased, non-transient friction coefficient magnitudes increase from values suggesting little solid contact to values indicating predominant metallic contact. For the physical

system of this investigation the trend means progressively less viscous action with increasing average speed. The reason for this effect might be found in the work of Bowden and Ridler [4] and of Jaeger [37], who has performed a thermodynamic analysis of the surface temperatures to be expected at asperity contacts under kinetic conditions. Jaeger's analysis, which ignored the thermal capacity of any lubricant present, yielded the result

$$T - T_\infty = \frac{\mu_k \, v \, N_s \, g \, b}{1.9 \, J \, A^{1/2} \left[1.1 \, \xi_2 b + 0.7 \, \xi_1 A^{1/4} v^{1/2} \right]} \,, \tag{5.2.1}$$

where

N_s = normal load carried by solid contact

g = acceleration of gravity

T_∞ = temperature at infinity

J = work equivalent of heat

ξ_1, ξ_2 = thermal conductivities of slider and lower surface, respectively

b = a ratio of material constants of the slider.

For a given pair of friction surfaces this equation may be reduced to

$$T - T_\infty = K \frac{\mu_k \, v \, N_s^{1/2}}{a + v^{1/2} N_s^{1/4}} \,. \tag{5.2.2}$$

Jaeger's results, derived for non-oscillatory sliding conditions, may not be directly applied to the present study, but general trends would still be analagous. Note that, for the present study, the average temperature of an asperity contact would therefore have increased with both driven surface velocity and the proportion of normal load supported by solid contact, which itself increased with driven surface velocity. Peak temperatures achieved can be very high [4,37]; the average temperature of the continuously-exposed upper surface, and with it the average temperature of the lubricant in the load-bearing region, could increase substantially with driven surface velocity, providing an explanation for the observed quasi-steady viscosity decreases.

Consider now the effect of increased surface temperatures on the elastohydrodynamic frictional traction curve (Figure 3.2.2). The conditions for which Crook's analytical expression, equation 3.2.4, was derived are not satisfied in this investigation, preventing an appeal to that established result. Heat was not generated exclusively in the lubricant, as in the elastohydrodynamic case; the lubricant may even have contributed to the cooling, rather than heating, of the solid surfaces. One can only again point out that the decrease in elastohydrodynamic friction force with increasing relative surface velocities is attributed to a thermal decrease in lubricant viscosity. That the maximum of an elastohydrodynamic friction force curve would occur at a

lower surface velocity for increased overall operating temperatures therefore offers an explanation for the appearance of such a maximum only with the high driven surface velocities of quasi-harmonic oscillation.

CHAPTER VI

VI. CONCLUSION

The interest of the present study was the influence of rate effects on static and dynamic boundary friction. An equation predicting the variation in the observed coefficient of static friction with load rate was developed from consideration of plastic flow, and the predicted behaviour compared to experimentally-obtained data. The dynamic frictional action encountered during quasi-harmonic oscillation and during the slip portion of the stick-slip vibration cycle was recorded and analyzed. In every case rate effects were found to determine or profoundly influence the observed frictional behaviour. In specific detail, the following conclusions may be listed:

1. The assumption of a plastic deformation model, for the growth in contact area of opposing surfaces subject to normal and tangential loading, permitted development of an equation predicting the variation of the coefficient of static friction with rate of stress application. Within the limits of scatter of experimental data, the profile of the equation's plotted curve matches the profile of the plotted data. The compatibility of these profiles suggests strongly that plastic deformation is indeed the governing mechanism of contact area growth between metal surfaces.

2. The existence of an upper asymptote for static friction of metallic surfaces, at slow rates of loading and in the presence of a lubricant, has been proven.

3. The kinetic friction force vs velocity curve for stick-slip oscillation of metallic surfaces has been proven to consist of two regimes, transient and steady-state.

4. Decay of the transient portion of the stick-slip friction vs velocity curve to the steady-state kinetic friction curve appears to be governed by the distance travelled, subsequent to the inception of slip, by one surface over the other.

5. The steady-state portion of the kinetic friction curve for slip exhibits definite characteristics of both viscous and metallic solid-contact behaviour.

6. The viscous contribution to the dynamic frictional behaviour became increasingly smaller as the average relative velocity of the friction surfaces increased, apparently because the temperature of the lubricant in the load-bearing interfacial region increased, and its viscosity decreased, as average surface velocity increased.

7. Comparison of recorded kinetic friction vs relative velocity curves from quasi-harmonic oscillation and elastohydrodynamic lubrication investigations indicates

that the observed frictional behaviour causing quasi-harmonic oscillation is the result of superimposed metallic solid-contact and elastohydrodynamic effects.

8. Non-oscillatory slip and quasi-harmonic oscillation would therefore, in a physical system, appear to be distinct entities only because, in the case of quasi-harmonic oscillation, instantaneous viscous thermal effects are sufficiently severe to cause a "humped" form of friction force vs relative velocity curve.

APPENDICES

APPENDIX I

SYSTEM PARAMETERS

A1.1 System Stiffness

For the composite beam of Figure A1.1, which approximates the cantilever beam employed in the experimental system, deflection and slope at pt. a due to a force P acting at pt. b are [38]

$$\delta_a = \frac{1}{3}\frac{PL_1^3}{E_1I_1} + \frac{1}{2}\frac{PL_2L_1^2}{E_1I_1} = \frac{1}{3}\frac{PL_1^3}{E_1I_1}\left[1 + \frac{3}{2}\frac{L_2}{L_1}\right] ,$$

$$\theta_a = \frac{1}{2}\frac{PL_1^2}{E_1I_1} + \frac{PL_2L_1}{E_1I_1} = \frac{1}{3}\frac{PL_1^3}{E_1I_1}\frac{1}{L_2}\left[\frac{3}{2}\frac{L_2}{L_1} + 3\frac{L_2^2}{L_1^2}\right] .$$

Deflection at pt. b due to a force P acting at pt. b is, for small deflections,

$$\delta_b = \delta_a + \theta_a L_2 + \frac{1}{3}\frac{PL_2^3}{E_2I_2}$$

$$= \frac{1}{3}\frac{PL_1^3}{E_1I_1}\left[1 + 3\frac{L_2}{L_1} + 3\frac{L_2^2}{L_1^2}\right] + \frac{1}{3}\frac{PL_2^3}{E_2I_2} .$$

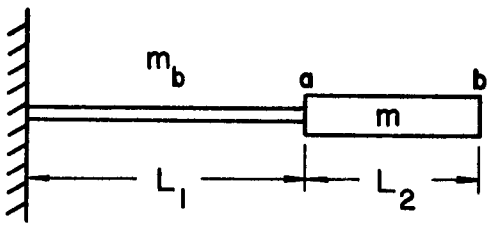

$L_1 = 7\frac{1}{8}"$ $\quad E_1 = 30 \times 10^6$ lb/in2 $\quad I_1 = 1.30 \times 10^{-3}$ in^4

$L_2 = 5\frac{3}{8}"$ $\quad E_2 = 10 \times 10^6$ lb/in2 $\quad I_2 = 3.38 \times 10^{-2}$ in^4

$$m_b = \frac{0.48 \text{ lb}}{g} \qquad m = \frac{1.90 \text{ lb}}{g}$$

Figure A1.1 Approximation of Composite Beam Employed for Analysis of Beam Properties

The stiffness of the composite cantilever beam was therefore estimated to be

$$k = \frac{P}{\delta_b} = \left[\frac{1}{3} \frac{L_1^3}{E_1 I_1} \left[1 + 3 \frac{L_2}{L_1} + 3 \frac{L_2^2}{L_1^2} \right] + \frac{1}{3} \frac{L_2^3}{E_2 I_2} \right]^{-1}$$

$$\cong 64 \frac{lb}{in} \quad .$$

The undamped natural frequency of the system may be estimated from the equation [39]

$$\omega_n \cong \left[\frac{k}{m} \right]^{\frac{1}{2}} \left[1 - \frac{33 m_b}{280\ m} \right] = 110 \frac{rad}{sec} \quad .$$

Measured values of system stiffness and frequency of free vibration were, respectively,

$$k = 59.2 \frac{lb}{in} \quad , \qquad \omega_d = 102 \frac{rad}{sec} \quad .$$

A1.2 System Damping

The equation of motion for a linear system in free vibration is

$$M \ddot{x} + r \dot{x} + k x = 0 \quad .$$

A solution for this differential equation is [40]

$$x = x_0 e^{-\frac{r}{2M}t} \sin(\omega_d t + \theta) \quad ,$$

where x_0 is the initial condition. If the time axis is oriented such that maximum positive displacement peaks occur when $(\omega_d t + \theta) = \frac{\pi}{2}(1 + 4n)$, then for these displacement peaks

$$x_n = x_0 e^{-\frac{r}{2M}nT}$$

where T is the period of one cycle of vibration, and consequently

$$r = \frac{2M}{nT} \ln \frac{x_0}{x_n} \quad .$$

Measurement of vibration amplitudes several cycles apart will therefore yield the value of the linear damping coefficient, but the value of M, the equivalent mass of the system, must first be determined by use of the equation

$$\omega_d = \sqrt{\frac{k}{M} - \left[\frac{r}{2M}\right]^2} \quad .$$

Combination of the two previous equations yields

$$M = \frac{k}{\omega_d^2 + \left[\frac{1}{nT} \ln \frac{x_0}{x_n}\right]^2} ,$$

enabling the determination of M directly, since all variables on the right-hand side of the equation were found by measurements performed on the system.

Recorded curves of displacement versus time were found to be only slightly non-linear, with an averaged decay coefficient

$$\frac{1}{nT} \ln \frac{x_0}{x_n} = 0.87 \text{ sec}^{-1} .$$

Substitution in the previous equations yields

$$M = 5.70 \times 10^{-3} \frac{\text{lb-sec}^2}{\text{in}} = \frac{2.20 \text{ lb}}{\text{g}}$$

$$r = 0.99 \times 10^{-2} \frac{\text{lb-sec}}{\text{in}}$$

For purposes of comparison, the critical damping coefficient and the undamped natural frequency of the vibratory system are, respectively,

$$r_c = 2\sqrt{k\,M} = 1.16 \frac{\text{lb-sec}}{\text{in}} ,$$

$$\omega_n = \sqrt{\frac{k}{M}} = 102 \frac{\text{rad}}{\text{sec}} .$$

APPENDIX II

PHASE PLANE ANALYSIS OF VIBRATORY MOTION

The popularly-designated "phase plane" is a plot of a differential equation's zeroth derivative of the dependent variable versus the first derivative of the dependent variable. The chief advantage of employing such a plot is that in the case of autonomous second-order differential equations, in which the independent variable found in the denominator of a derivative (eg. time) appears only in the denominator of a derivative, this independent variable is not explicitly expressed on the phase plane; rather, the interaction of the zeroth and first derivatives of the dependent variable is explored. A lesser benefit derived is that conversion of a second-order equation to phase plane form reduces it to simpler, first-order, form.

Consider, for example, the differential equation governing the motion of a mass restrained by an ideal spring.

$$M\ddot{x} + k\,x = 0$$

Conversion of the equation to phase plane form is accomplished through use of the following identity.

$$\ddot{x} = \frac{d}{dt}(\dot{x}) = \frac{d\dot{x}}{dx}\frac{dx}{dt} = \dot{x}\frac{d\dot{x}}{dx}$$

Substitution in the equation of motion yields

$$\frac{d\dot{x}}{dx} + \frac{k}{M}\frac{x}{\dot{x}} = 0 \quad ,$$

which may be integrated by separation of variables to obtain the solution

$$x^2 + \frac{M}{k}\dot{x}^2 = \text{constant} \quad ,$$

where the value of the constant is determined by initial conditions. This solution, if plotted on x and $\dot{x}$ co-ordinates, is obviously an ellipse. However, since $\left[\frac{k}{M}\right]^{1/2}$ defines the natural frequency of vibration of the system, the solution becomes a circle when plotted on the normalized co-ordinates x and $\frac{\dot{x}}{\omega_n}$.

Inclusion of a viscous damping term in the equation of motion gives it the form

$$M\ddot{x} + r\dot{x} + kx = 0 \quad ,$$

which when converted to phase plane form becomes

$$\frac{d\dot{x}}{dx} + \frac{k}{M}\frac{x}{\dot{x}} = -\frac{r}{M} \quad ,$$

with the viscous damping coefficient serving as a negative forcing function. The solution of this equation is a circular, decaying spiral when plotted on normalized phase plane co-ordinates. Of particular interest is the line called the "zero isocline", defined by the simultaneous validity of the phase plane form of the equation of motion and the condition

$$\frac{d\dot{x}}{dx} = 0 \quad .$$

For the case of free vibration with viscous damping the zero isocline is a straight line through the origin, with slope $-\frac{\omega_n}{k} r$ when plotted on the normalized phase plane.

Generally the zero isocline is a line which is neither straight nor passing through the origin. Its importance lies in the fact that the phase plane behavioural curve described by the equation of motion can be readily generated, by graphical means, from the zero isocline [41]. An example of a phase plane curve, for the case of free vibration with viscous damping, generated graphically from the zero isocline, is shown in Figure A2.1.

A line drawn through the intersection of the zero isocline and the zero velocity axis, perpendicular to the zero velocity axis, subdivides the phase plane into energy-additive and energy-dissipative quadrants. For the axes presented in this study, any portion of the zero isocline

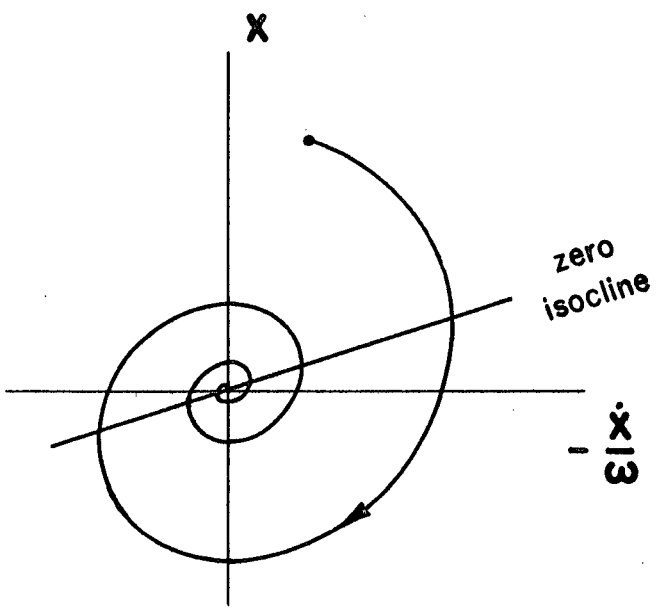

Figure A2.1 Viscously-Damped Free Vibration on Phase Plane

in the right upper or left lower energy-transfer quadrants is dissipative; any portion of the zero isocline in the left upper or right lower quadrants is energy-additive. The phase plane example of Figure A2.1 displays a zero isocline which is entirely energy-dissipative, because this isocline is totally contained in the upper right and lower left energy-transfer quadrants.

For the present study, as consultation of equation 4.2.3 will show, the zero isocline was the graph of the friction force experienced by the slider at the friction interface, divided by the system stiffness, plotted as a function of $\frac{v}{\omega_n}$. Simultaneous recording of the zero isocline and the phase plane behavioural trace therefore permitted the validity of the recorded friction curves to be tested (Fig. A2.2). More important, recording data in phase plane form has the advantage that the slip portion of a stick-slip cycle has consistently excellent resolution of detail on the phase plane. As a consequence of technical difficulties, such resolution is virtually unattainable in the time domain.

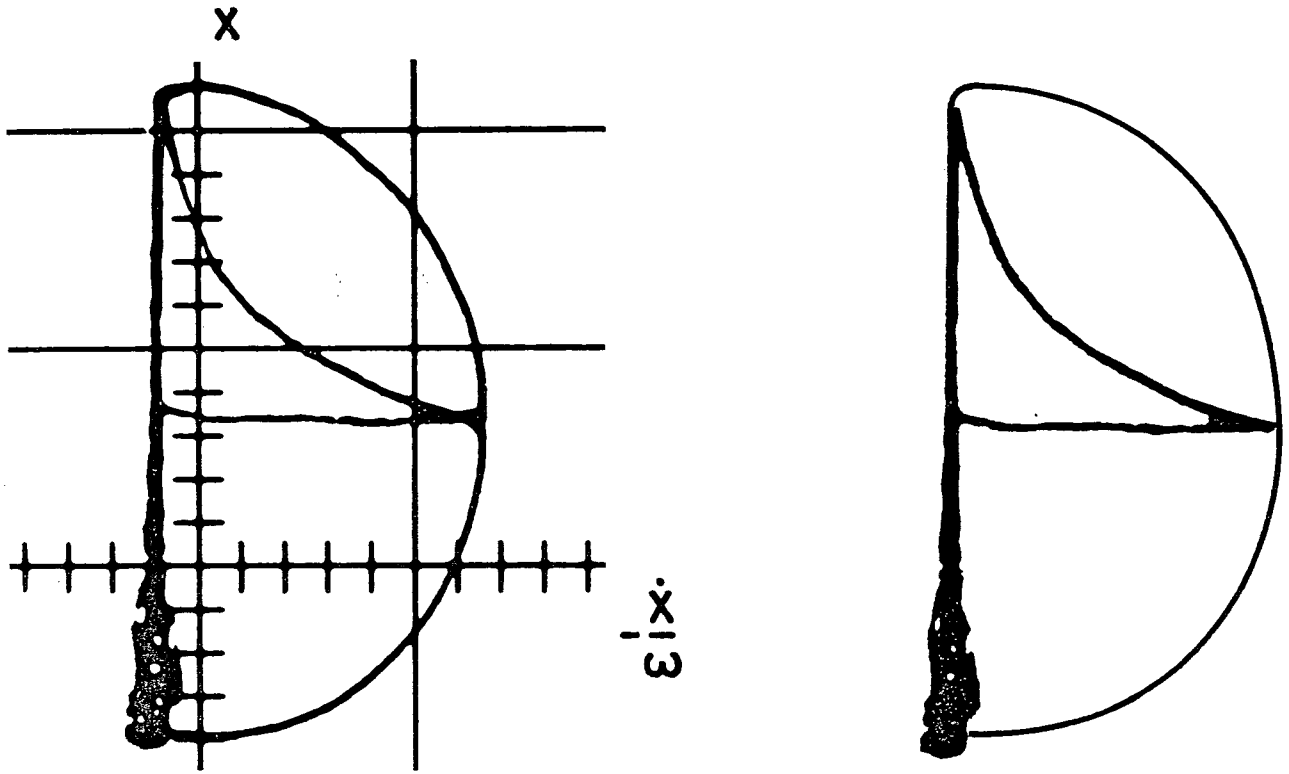

Figure A2.2 Comparison of Recorded and Graphically Generated Phase Plane Behavioural Traces

APPENDIX III

VISCOUS SQUEEZE FILM ANALYSIS

Consider the general form of Reynolds' equation,

$$\frac{\partial}{\partial x}\left[\frac{h^3}{\eta}\frac{\partial p}{\partial x}\right] + \frac{\partial}{\partial z}\left[\frac{h^3}{\eta}\frac{\partial p}{\partial z}\right] = 6\,U\,\frac{\partial h}{\partial x} + 6\,h\,\frac{\partial U}{\partial x} + 12\,\frac{dh}{dt} \quad ,$$

where the co-ordinates are as defined in Figure A3.1. For parallel surfaces separated by a constant-viscosity fluid, so that h and η are independent of x and z,

$$\frac{\partial^2 p}{\partial x^2} + \frac{\partial^2 p}{\partial z^2} = \nabla^2 p = \frac{12\eta}{h^3}\frac{dh}{dt} \quad .$$

For convenience, since in this study a circular slider face was employed, the Laplacian operator ∇^2 may be expressed in cylindrical co-ordinates, so that the equation in orthogonal components is altered to

$$\frac{1}{\rho}\frac{\partial}{\partial \rho}\left[\rho\,\frac{\partial p}{\partial \rho}\right] + \frac{1}{\rho^2}\frac{\partial^2 p}{\partial \theta^2} + \frac{\partial^2 p}{\partial y^2} = \nabla^2 p = \frac{12\eta}{h^3}\frac{dh}{dt} \quad .$$

The quantities $\frac{\partial^2 p}{\partial \theta^2}$ and $\frac{\partial^2 p}{\partial y^2}$ may be equated to zero from considerations of symmetry and thin-film approximations, respec-

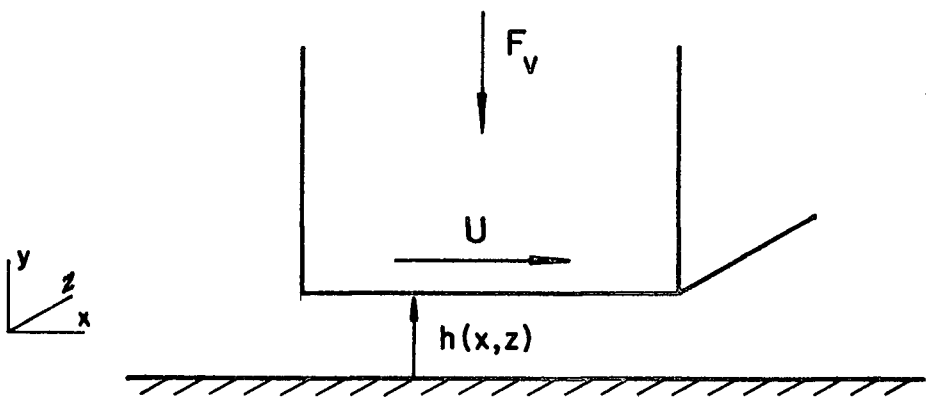

Figure A3.1 Squeeze Film Analysis Co-ordinates

tively, leaving the relationship

$$\frac{1}{\rho}\frac{d}{d\rho}\left[\rho\frac{dp}{d\rho}\right] = \frac{12\eta}{h^3}\frac{dh}{dt} \quad .$$

Integrating twice, and solving for the boundary conditions

$$p = 0, \qquad \rho = R$$

$$\frac{dp}{d\rho} = 0, \qquad \rho = 0$$

yields

$$p = \frac{3\eta}{h^3}(\rho^2 - R^2)\frac{dh}{dt} \quad .$$

Integrating the pressure distribution over the surface area of the slider results in an expression for the normal load supported by fluid pressure,

$$N_f = \int_{\rho=0}^{\rho=R} p \cdot 2\pi\rho \, d\rho = -\frac{3}{2}\pi\eta R^4 \cdot \frac{1}{h^3}\frac{dh}{dt} \quad .$$

Note that the form of this expression is such that, for a constant normal load, the rate of decrease of the film thickness diminishes with the third power of the film thick-

ness. For plane surfaces the film thickness can be reduced to zero only as time or normal load assumes an infinite value. Real surfaces, which are not planar, cannot reduce the mean film thickness to zero, but the load-bearing capacity of the film is still governed by the expression for N_f if the planar film thickness h is replaced by its effective counterpart.

APPENDIX IV

CALIBRATION AND SCALING OF DISPLACEMENT, VELOCITY, AND FRICTION FORCE SIGNALS

A4.1 Scaling of Displacement and Velocity Signals

The accelerometer employed was a commercial unit with a fixed output voltage equal to 0.1 volts per unit gravity. This output, which was readily checked at any time, was used as a standard calibration reference for the displacement and velocity signals.

The displacement signal was scaled simply by subjecting the cantilever beam, complete with all instrumentation, slider, and slider mount, to conditions of free vibration, and adjusting the magnitude of the displacement signal until, at zero velocity, the sum of the displacement and acceleration signals equaled zero. Because the viscous damping effect was so small, this procedure resulted in the summed signal taking the form of a straight line whose slope, on the face of an oscilloscope, was indistinguishable from that of the zero displacement.

Upon achieving the proper magnitude of displacement signal, the velocity signal strength was adjusted until the system's phase plane trace, as recorded by an oscilloscope, was a circular, as opposed to ellipsoidal, spiral. That the

trace was a multi-cycle spiral, rather than a repetitive loop, is due to the small amount of near-linear viscous damping present under conditions of free vibration.

A4.2 Calibration of Displacement, Velocity, and Friction Force Signals

After the displacement signal was properly scaled a depth micrometer was rigidly mounted with its spindle in the horizontal plane and perpendicular to the side of the slider mount. Voltage output from the strain gage bridge was plotted against displacements imposed at the slider mount by the micrometer to obtain a calibration curve (Fig. A4.1). Deflections recorded on the oscilloscope were then readily converted to slider displacements.

Velocity calibration was inherent in the adjustment of velocity signal strength to achieve a circular form of phase plane trace in free vibration. One linear unit on the "velocity" axis is then equal to the displacement represented by that unit on the displacement axis multiplied by the natural frequency of vibration of the system, ω_n.

Calibration of the oscilloscope friction force trace was a simple matter of multiplying the oscilloscope displacement calibration by the system stiffness k.

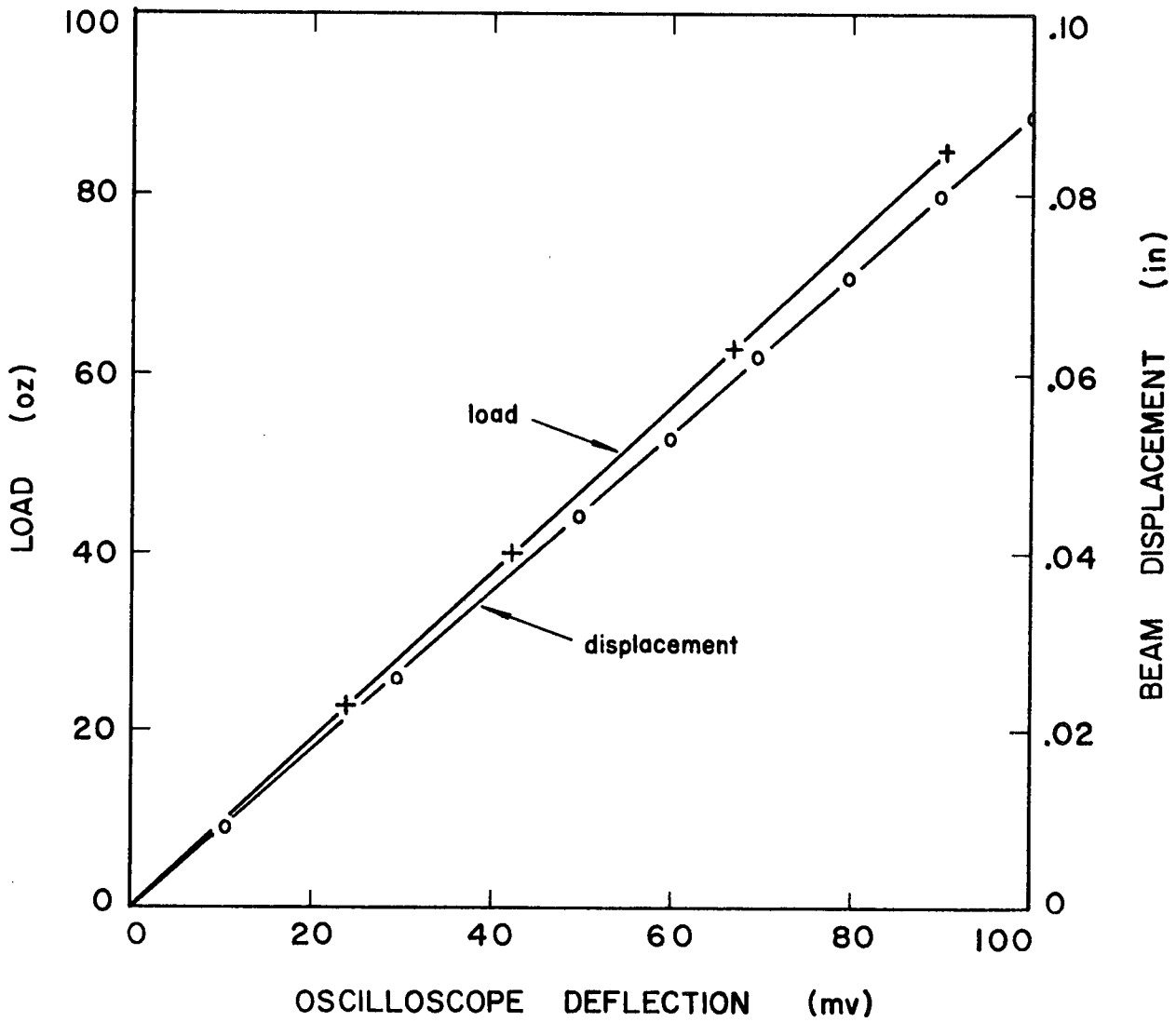

Figure A4.1 Calibration Curves for Composite Beam and Scaled Displacement Amplifier

APPENDIX V

FRICTION SURFACE PARAMETERS

Surface Roughness

	Surface	Roughness Along Directional Marks	Roughness Across Directional Marks
Lapped Surface Measurements	Steel Slider	18 µin. CLA	
	Steel Disc	18 µin. CLA	
Post-Test Measurements	Steel Slider	1-1$\frac{1}{2}$ µin. CLA	3 µin. CLA
	Steel Disc	13 µin. CLA	14 µin. CLA

(Measurements made with Talysurf 4 equipment)

Surface Composition and Hardness

	Composition and Condition	Indentation Hardness ($\frac{1}{16}$" dia.ball)
Steel Disc	mild steel, AISI C1020 fully annealed	Brinell 120
Steel Slider	alloy steel (C 1.05%, Mn 0.20%, Si 0.20%) as delivered	Brinell 235
Brass Slider	unleaded brass (Cu 70%, Zn 30%) as delivered	Brinell 165

REFERENCES

REFERENCES

1. Thomas, S. "Vibrations Damped by Solid Friction", The Philosophical Magazine, Series 7, Vol. 9, p. 329, 1930.

2. Papenhuyzen, P.J. "Wrijvings Proeven in Verbandmet het Slippen Van Autobanden", De Ingenieur, 53, p. 75, 1938.

3. Bowden, F.P. and Leben, L. "The Nature of Sliding and the Analysis of Friction", Proceedings of the Royal Society (London), A169, p. 371, 1939.

4. Bowden, F.P. and Ridler, K.E.W. "Physical Properties of Surfaces", Proceedings of the Royal Society (London), A151, p. 610, 1936.

5. Bristow, J.R. "Kinetic Boundary Friction", Proceedings of the Royal Society (London), A189, p. 88, 1945.

6. Dudley, B.R. and Swift, H.W. "Frictional Relaxation Oscillations", The Philosophical Magazine, Series 7, Vol. 40, p. 849, 1949.

7. Bowden, F.P. and Tabor, D. The Friction and Lubrication of Solids, Clarendon Press, pp. 10-32, 1950.

8. Rabinowicz, E. "A Study of the Stick-Slip Process", Proceedings of the Symposium on Friction and Wear, Detroit, 1957.

9. Courtney-Pratt, J.S. and Eisner, E. "The Effect of a Tangential Force on the Contact of Metallic Bodies", Proceedings of the Royal Society (London), A238, p. 529, 1957.

10. Potter, A.F. "A Study of Friction Induced Vibration", M.A.Sc. Thesis, Dept. of Mechanical Engineering, U.B.C., 1962.

11. Cameron, R. "Friction Induced Vibration", M.A.Sc. Thesis, Dept. of Mechanical Engineering, U.B.C., 1963.

12. Bell, R. and Burdekin, M. "Dynamic Behaviour of Plain Slideways", Proceedings of the Institution of Mechanical Engineers, Vol. 181, Part 1, No. 8, p. 169, 1966.

13. Davis, H.R. "The Dependence of the Static Coefficient of Friction on the Time of Stationary Contact", M.A.Sc. Thesis, Dept. of Mechanical Engineering, U.B.C., 1969.

14. Johannes, V.I. "Friction Induced Vibrations in a Hydraulically Driven System", Ph.D. Thesis, Dept. of Mechanical Engineering, U.B.C., 1969.

15. Ko, P.L. "Autonomous Quasi-Harmonic and Forced Vibration of Frictional Systems", Ph.D. Thesis, Dept. of Mechanical Engineering, U.B.C., 1969.

16. Green, M.A. "Some Fundamental Aspects of Static Friction", M.A.Sc. Thesis, Dept. of Mechanical Engineering, U.B.C., 1971.

17. Derjaguin, B.V., Push, V.E. and Tolstoi, D.M. "A Theory of Stick-Slip Sliding of Solids", Proceedings of the Conference of Lubrication and Wear, London, p. 265, 1957.

18. Kosterin, J.I. and Kragelskii, I.V. "Rheological Phenomena in Dry Friction", Wear, Vol. 5, p. 190, 1962.

19. Greenwood, J.A. and Williamson, J.B.P. "Contact of Nominally Flat Surfaces", Proceedings of the Royal Society (London), Vol. A295, p. 300, 1966.

20. McFarlane, J.S. and Tabor, D. "Relation Between Friction and Adhesion", Proceedings of the Royal Society (London), A202, p. 244, 1950.

21. Parker, R.C. and Hatch D. "The Static Coefficient of Friction and the Area of Contact", Proceedings of the Physical Society (London), B63, p. 185, 1950.

22. Tabor, D. "Junction Growth in Metallic Friction: The Role of Combined Stresses and Surface Contamination", Proceedings of the Royal Society (London), Vol. A251, p. 378, 1959.

23. Tabor, D. The Hardness of Metals, Clarendon Press, 1951.

24. Polakowski, N.H. and Ripling, E.J. Strength and Structure of Engineering Materials, Prentice-Hall, p. 217, 1966.

25. Atkins, A.G., Silverio, A. and Tabor D. "Indentation Hardness and the Creep of Solids", Journal of the Institute of Metals, Vol. 94, p. 369, 1966.

26. Bowden, F.P. and Young, J.E. "Friction of Clean Metals and the Influence of Adsorbed Films", Proceedings of the Royal Society (London), Vol. A208, p. 311, 1951.

27. Nadai, A. and Majoine, M.J. "High-Speed Tension Tests at Elevated Temperatures", Transactions of the American Society of Mechanical Engineers, Vol. 63, p. A77, 1941.

28. McClintock, F.A. and Argon, A.S. Mechanical Behaviour of Materials, Addison-Wesley, pp. 626-645, 1966.

29. Brown, E.D., Owens, R.S. and Booser, E.R. "Friction of Dry Surfaces", Boundary Lubrication - An Appraisal of World Literature, The American Society of Mechanical Engineers, pp. 7-16, 1969.

30. Barwell, F.T. Lubrication of Bearings, Butterworths Scientific Publications, p. 226, 1956.

31. Kannel, J.W. "Measurements of Pressures in Rolling Contact", Symposium on Elastohydrodynamic Lubrication, Proceedings of the Institution of Mechanical Engineers, Vol. 180, Part 3B, pp. 135-142, 1965.

32. Crook, A.W. "The Lubrication of Rollers; III - A Theoretical Discussion of Friction and the Temperatures in the Oil Film", Philosophical Transactions of the Royal Society (London), Vol. A254, p. 237, 1961.

33. Fridman, H.D. and Levesque, P. "Reduction of Static Friction by Sonic Vibrations", Journal of Applied Physics, Vol. 30, No. 10, p. 1572, 1959.

34. Beare, W.G. and Bowden, F.P. "Physical Properties of Surfaces: I - Kinetic Friction", Philosophical Transactions of the Royal Society (London), Vol A234, p. 329, 1935.

35. Haviland, M.L. and Rogers, J.J. "Friction Characteristics of Automatic Transmission Fluids as Related to Transmission Operation", Lubrication Engineering, Vol. 17, No. 3, p. 110, 1961.

36. Sprague, S.R. and Cunningham, R.G. "Frictional Characteristics of Lubricants", Industrial and Engineering Chemistry, Vol. 51, No. 9, p. 1047, 1959.

37. Jaeger, J.C. "Moving Sources of Heat and the Temperature at Sliding Contacts", Journal and Proceedings of the Royal Society of New South Wales, Vol. 76, p. 203, 1942.

38. Singer, F.L. Strength of Materials, Harper and Row, Second Edition, pp. 183-192, 1951.

39. McLachlan, N.W. Theory of Vibrations, Dover Publications, p. 12, 1951.

40. Wylie, C.R. Advanced Engineering Mathematics, Second Edition, McGraw-Hill, pp. 201-213, 1960.

41. Cunningham, W.J. Introduction to Nonlinear Analysis, McGraw-Hill, pp. 32-48, 1958.

42. Dowson, D. "Elastohydrodynamic Lubrication: An Introduction and a Review of Theoretical Studies", Symposium on Elastohydrodynamic Lubrication, Proceedings of the Institution of Mechanical Engineers, Vol. 180, Part 3B, p. 11, 1965.

43. Crook, A.W. "The Lubrication of Rollers: IV - Measurements of Friction and Effective Viscosity", Philosophical Transactions of the Royal Society (London), Vol. A255, p. 300, 1962.

44. Samuels, L.E. and Mulhearn, T.O. "An Experimental Investigation of the Deformed Zone Associated with Indentation Hardness Impressions", Journal of the Mechanics and Physics of Solids, Vol. 5, p. 125, 1956.

45. Bowden, F.P. and Tabor, D. The Friction and Lubrication of Solids, Vol. II, Clarendon Press, p. 72, 1964.